UNIVERSITY OF CALIFORNIA, SAN DIEGO

# Role of Apolipoprotein A-I Binding Protein in Regulation of Inflammation and Metabolism

A dissertation submitted in partial satisfaction of the degree requirements for the degree Doctor of Philosophy

in

Biomedical Sciences

by

Dina Allison Schneider

Committee in charge:

Professor Yury Miller, Chair
Professor Jack Bui
Professor Christopher Glass
Professor Judith Varner
Professor Joseph Witztum

2018

The Dissertation of Dina Allison Schneider is approved, and it is acceptable in quality and form for publication on microfilm and electronically:

---

---

---

---

---

Chair

University of California, San Diego

2018

# DEDICATION

This dissertation is dedicated to my family, for inspiring me to never stop learning.

TABLE OF CONTENTS

# LIST OF ABBREVIATIONS

ABC: ATP Binding Cassette

AIBP: Apolipoprotein A-I Binding Protein

CVD: Cardiovascular Disease

HDL: High Density Lipoprotein

HFC: High Fat & Cholesterol diet

HFD: High Fat Diet

LDL: Low Density Lipoprotein

LPS: Lipopolysaccharide

OXPHOS: Oxidative Phosphorylation

RCT: Reverse Cholesterol Transport

VLDL: Very Low Density Lipoprotein

WD: Western Diet

LIST OF FIGURES

LIST OF TABLES

ACKNOWLEDGMENTS

I would like to acknowledge my coauthors Soo-Ho Choi, Colin Agatisa-Boyle, Laurence Zhu, Jungsu Kim, Jennifer Pattison, Dorothy D. Sears, Philip L.S.M. Gordts, Longhou Fang, and Yury I. Miller for their contributions to Chapter 1, as well as the publishing journal The Journal of Lipid Research.

I would also like to thank my family, friends, and labmates for their support and encouragement during my PhD. This work would not be possible without them. I would especially like to thank my advisor Dr. Yury Miller for his continued guidance and mentorship. My time in Yury's lab has shaped me into the scientist I am today.

Chapter 1, in full, is a reprint of the material as it appears in The Journal of Lipid Research 2018. Schneider, Dina A.; Choi, Soo-Ho; Agatisa-Boyle, Colin; Zhu, Laurence; Kim, Jungsu; Pattison, Jennifer; Sears, Dorothy D.; Gordts, Philip L.S.M.; Fang, Longhou; Miller, Yury I., The American Society for Biochemistry and Molecular Biology, 2018. The dissertation author was the primary investigator and author of this paper.

# VITA

| | |
|---|---|
| 2010-2012 | Research Assistant, United States Department of Agriculture |
| 2012 | Bachelor of Science, University of California, Davis |
| 2018 | Doctor of Philosophy, University of California, San Diego |

ABSTRACT OF THE DISSERTATION

Role of Apolipoprotein A-I Binding Protein in Regulation of Inflammation and Metabolism

by

Dina Allison Schneider

Doctor of Philosophy in Biomedical Sciences

University of California, San Diego, 2018

Professor Yury Miller, Chair

Despite being discovered nearly two decades ago, little is known about the *in vivo* function of Apolipoprotein A-I Binding Protein (AIBP). The aim of our studies was to determine this function through the use of loss-of-function knockout models and gain-of-function overexpression models. We found that AIBP plays a protective role against atherosclerosis and inflammation, by enhancing cholesterol efflux from the vessel wall and preventing inflammatory macrophage signaling. It also appears to regulate whole-body metabolism, possibly via a

different mechanism. Intriguingly, while AIBP is protective against certain conditions, it may actually be detrimental to cancer survival. Tumors express AIBP, and mice lacking AIBP expression had slower sarcoma growth than wildtype mice. Taken together, these data show that AIBP has important *in vivo* functions in a variety of pathologies.

# INTRODUCTION

## *Apolipoprotein A-I Binding Protein*

Apolipoprotein A-I Binding Protein (AIBP) is a recently characterized protein, first discovered in a 2002 human liver yeast two-hybrid screen for ApoA-I interactors (Ritter, Buechler et al. 2002). It is highly conserved across species, with 88.2% homology between mouse and human (Ritter, Buechler et al. 2002). Expression levels vary across tissues, with kidney, heart, liver, thyroid, adrenal glands, and testis containing the highest mRNA content, and cellular localization varies as well (Ritter, Buechler et al. 2002). AIBP can be found in the nucleus, cytosol, and mitochondria, and is also secreted, leading to its expression in the plasma, cerebrospinal fluid, and urine of certain individuals (Ritter, Buechler et al. 2002). Secretion appears to be regulated by external stimuli, to date only stimulation of kidney proximal tubule cell secretion by ApoA-I or HDL have been published as triggers (Ritter, Buechler et al. 2002).

The protein itself is approximately 29 kDa, and the *Apoa1bp* gene is 2.5 kb, comprising 6 exons and 5 introns (Ritter, Buechler et al. 2002). AIBP contains a YjeF_N domain, whose function is poorly understood (Rudolph, Sigruener et al. 2007). The protein can be both phosphorylated and lysine-acetylated (Jha, Shumilin et al. 2008, Zhang, Zhao et al. 2010). Two forms of AIBP are produced either including or excluding a signal sequence, dependent upon where transcription is initiated from (Marbaix, Tyteca et al. 2014). This sequence has been predicted to be a signal peptide and/or a mitochondrial pro-peptide in the current literature, although controversy exists over its true function (Ritter, Buechler et al. 2002, Marbaix, Tyteca et al. 2014).

The structure of AIBP predicts enzymatic activity involving a nucleotide substrate or cofactor, but characterization of this function warrants further study (Jha, Shumilin et al. 2008,

Shumilin, Cymborowski et al. 2012). Several papers have proposed a role for AIBP in nicotinamide nucleotide repair as an epimerase of hydrated NAD(P)H (Marbaix, Noel et al. 2011, Kremer, Danhauser et al. 2016), and metabolite cocktail screenings reveal that AIBP is able to bind NAD(P) and NAD(P)H (Shumilin, Cymborowski et al. 2012). From structural data, a function as an ADP-ribosyltransferase has also been proposed, (Shumilin, Cymborowski et al. 2012) although conclusive data has yet to be published.

Secreted, extracellular AIBP has a functional role in cholesterol efflux, the process whereby excess cholesterol is removed from cells in the periphery (Jha, Shumilin et al. 2008, Fang, Choi et al. 2013, Mao, Meng et al. 2017). AIBP enhances cholesterol efflux from cells to HDL or ApoA-I and increases their ability to bind to cells, but is not itself a cholesterol acceptor (Fang, Choi et al. 2013). Additionally, AIBP has the ability to bind ABCA1, an ATP-Binding Cassette (ABC) transporter which facilitates cholesterol efflux from the cell (Zhang, Li et al. 2016). As a result of these interactions, lipid raft content in targeted cells is reduced, and downstream raft-mediated signaling is suppressed (Fang, Choi et al. 2013, Mao, Meng et al. 2017). This mechanism has been predicted or shown to have significance in numerous cell types, including sperm, endothelial cells, and macrophages (Jha, Shumilin et al. 2008, Fang, Choi et al. 2013, Zhang, Li et al. 2016).

*Lipid Rafts & Cholesterol Homeostasis*

Lipid rafts are microdomains in the plasma membrane which are enriched in cholesterol and sphingomyelin. Rafts serve as an ordered membrane environment and signaling platform for numerous signal transduction mechanisms, including inflammatory pathways (Triantafilou, Miyake et al. 2002, Patel and Insel 2009). Treatment with lipopolysaccharide (LPS), an

inflammatory component of gram-negative bacterial membranes, induces lipid raft recruitment of Toll-Like Receptor 4 (TLR4) and its associated downstream signaling (Triantafilou, Miyake et al. 2002). Intriguingly, membrane cholesterol loading alone is enough to activate TLR4 signaling, emphasizing the importance of cholesterol regulation and homeostasis (Fessler and Parks 2011).

Cellular cholesterol content is highly regulated. Excess cholesterol is removed from cells via the process of Reverse Cholesterol Transport (RCT). In RCT, ApoA-I and HDL circulate and collect cholesterol from peripheral tissues via efflux, which is transported to the liver for conversion to bile and eventual excretion (Tall and Yvan-Charvet 2015). HDL-mediated cholesterol efflux is able to prevent atherogenic vascular lipid accumulation and arterial inflammation (Tall and Yvan-Charvet 2015).

*Relevance of AIBP in Macrophage Polarization*

Work from our lab and others has recently shown that in addition to endothelial cells, AIBP can mediate cholesterol efflux from macrophages (Fang, Choi et al. 2013, Zhang, Li et al. 2016). Importantly, the ability of AIBP to regulate lipid raft content may have broad implications for macrophage polarization and its associated pathologies.

Macrophages exhibit a spectrum of functional phenotypes. The most well-characterized are the pro-inflammatory classically-activated M1 and anti-inflammatory alternatively-activated M2, although these descriptors should be considered a useful paradigm rather than an exact representation of *in vivo* macrophages. The M1 and M2 descriptors are derived from their functional association with T helper cell subsets $T_H1$ and $T_H2$ respectively (Lawrence and Natoli 2011). Other stimuli can also influence macrophage polarization, including lipopolysaccharide

(LPS) and IFNγ for M1 and IL-4, IL-13, IL-10, glucocorticoids, and TGFβ for M2 (Martinez, Sica et al. 2008). M-CSF, a driver of monocyte-to-macrophage differentiation, produces a similar transcriptome to that of M2 macrophages, suggesting that M2 is the default polarization (Martinez, Gordon et al. 2006). Several other subsets have been identified in atherosclerotic lesions including M(Hb), Mhem, M4, and Mox, but the functionality of these other subsets in atherosclerosis progression is still unclear (Chinetti-Gbaguidi, Colin et al. 2015).

The signaling pathways that drive macrophage polarization are complex. Interestingly, M1 polarization is primarily regulated by activation of TLR4 and IFNGR, receptors that localize to lipid rafts for their function (Lawrence and Natoli 2011, de Weerd and Nguyen 2012, Plociennikowska, Hromada-Judycka et al. 2015). M2 polarization is dependent on the IL-4 receptor, and mice with a myeloid-specific knockout of *Il4r* do not develop M2 macrophages (Lawrence and Natoli 2011). One report found that the IL-4Rα is present in human T cell raft fractions and another showed that raft disruption affects T cell responsiveness to IL-4, but there is no conclusive evidence that IL-4 signaling in macrophages is lipid raft-dependent (Rao, Logan et al. 2004). Thus, it appears that enhanced lipid raft presence in the plasma membrane is supportive of M1 but not necessarily M2 polarization. Further, this indicates that by reducing cellular lipid raft content, AIBP may inhibit an M1 state and resulting downstream inflammation.

*Macrophage Involvement in Disease*

Within atherosclerotic lesions, cholesterol crystals, oxidized lipoproteins, and inflammatory cytokines all induce M1 polarization, while IL-4 present in the plaque leads to M2 polarization (Chinetti-Gbaguidi, Colin et al. 2015). Plaque T helper cells secrete polarizing factors that also regulate the M1/M2 balance (Moore, Sheedy et al. 2013). Additionally, excess

plasma membrane cholesterol enrichment leads to sustained TLR4 signaling, and thus inflammation (Moore, Sheedy et al. 2013). Macrophage localization in the lesion is linked to polarization status; pro-inflammatory M1 macrophages tend to locate in the unstable shoulder region while anti-inflammatory M2 macrophages favor stable areas and asymptomatic lesions (Chinetti-Gbaguidi, Colin et al. 2015). Preclinical models predict that therapeutics altering the M1/M2 balance to favor M2 would be atheroprotective, indicating potential for AIBP as a novel therapy (Moore, Sheedy et al. 2013).

Insulin resistance and metabolic disease have been overwhelmingly linked to inflammation, with a high degree of macrophage involvement. Intriguingly, obesity is often associated with increased risk of other inflammatory conditions including CVD and cancer (Osborn and Olefsky 2012). Tracking experiments performed in the lab of Jerrold Olefsky elegantly showed that monocyte migration into adipose tissue is significantly greater in obese mice, and that under obesity conditions these cells polarize to an M1-like macrophage state (Oh, Morinaga et al. 2012). These experiments also showed that the cells of obese mice are not predisposed to an inflammatory state; instead tissue conditions polarize the macrophages (Oh, Morinaga et al. 2012). Lipid-overloaded adipocytes secrete chemokines such as MCP-1 that attract monocytes into the fat tissue, where they differentiate into macrophages and secrete their own chemokines, producing a feed-forward loop (Osborn and Olefsky 2012). Accordingly, obese adipose tissue can be composed of up to 40% adipose tissue macrophages (ATMs), which have been shown to be active secretors of pro-inflammatory cytokines (Osborn and Olefsky 2012).

Macrophage inflammation is critical to the development of insulin resistance. Targeted disruption of the inflammatory JNK signaling pathway in macrophages has been shown to protect against insulin resistance in mice, accompanied by a reduction in M1 macrophage

presence (Han, Jung et al. 2013). The level of M1-like ATMs has been shown to correlate with the degree of insulin resistance in an individual (Osborn and Olefsky 2012). ATMs in lean adipose tissue are primarily anti-inflammatory, so the shift to an M1 phenotype is notable (McNelis and Olefsky 2014). Inflammatory macrophage infiltration occurs in other tissues as well under metabolic disease conditions, especially the pancreas and liver (Odegaard and Chawla 2013).

Cancer is another pathology with a high degree of inflammatory contribution. Chronic inflammation has been shown to increase cancer risk, and immune cells are frequently found within tumors (Grivennikov, Greten et al. 2010). Interestingly, the chronic inflammatory condition of obesity has been found to promote liver cancer via IL-6 and TNFα (Park, Lee et al. 2010). However, an inflammatory M1 macrophage response can drive anti-tumor activity, so targeted intervention in the tumor immune contexture is complicated to perform (Biswas and Mantovani 2010).

Tumor-associated macrophages (TAMs) share many functions with M2 macrophages, but have a distinctly different transcriptome (Lawrence and Natoli 2011). TAMs primarily originate as circulating blood monocytes and are recruited to the tumor site by tumor-produced M-CSF, MCP-1, and other signals, although some reports indicate that they also arise from yolk sac progenitors and extramedullary hematopoiesis (Noy and Pollard 2014). Both M1 and M2 macrophages can be found in early-stage tumors, but tumor-secreted factors polarize the majority of TAMs to resemble an M2 phenotype by later stages (Bronte and Murray 2015). M2-like macrophages can perform several tumor-supportive functions; they increase invasiveness via production of matrix-remodeling proteins, promote neovascularization of the tumor, inhibit anti-tumor immune function, and promote tumor growth (Noy and Pollard 2014). TAMs also fail to

produce inflammatory cytokines and are not cytotoxic to tumor cells (Allavena, Sica et al. 2008). Currently no therapy exists to manipulate macrophage polarization within the tumor (Bronte and Murray 2015).

*Support for AIBP as a Potential Therapeutic*

Given the importance of macrophage-mediated inflammation across a variety of pathologies, our studies aimed to uncover the role that AIBP may play in several. AIBP is known to enhance cholesterol efflux from macrophages, but the functional consequences of this mechanism in disease are yet unknown (Zhang, Li et al. 2016). As a proposed suppressor of inflammatory macrophage polarization and signaling, AIBP may be a novel therapeutic target.

## References


Allavena, P., A. Sica, G. Solinas, C. Porta and A. Mantovani (2008). "The inflammatory micro-environment in tumor progression: the role of tumor-associated macrophages." Crit Rev Oncol Hematol **66**(1): 1-9.

Biswas, S. K. and A. Mantovani (2010). "Macrophage plasticity and interaction with lymphocyte subsets: cancer as a paradigm." Nat Immunol **11**(10): 889-896.

Bronte, V. and P. J. Murray (2015). "Understanding local macrophage phenotypes in disease: modulating macrophage function to treat cancer." Nat Med **21**(2): 117-119.

Chinetti-Gbaguidi, G., S. Colin and B. Staels (2015). "Macrophage subsets in atherosclerosis." Nat Rev Cardiol **12**(1): 10-17.

de Weerd, N. A. and T. Nguyen (2012). "The interferons and their receptors--distribution and regulation." Immunol Cell Biol **90**(5): 483-491.

Fang, L., S. H. Choi, J. S. Baek, C. Liu, F. Almazan, F. Ulrich, P. Wiesner, A. Taleb, E. Deer, J. Pattison, J. Torres-Vazquez, A. C. Li and Y. I. Miller (2013). "Control of angiogenesis by AIBP-mediated cholesterol efflux." Nature **498**(7452): 118-122.

Fessler, M. B. and J. S. Parks (2011). "Intracellular lipid flux and membrane microdomains as organizing principles in inflammatory cell signaling." J Immunol **187**(4): 1529-1535.

Grivennikov, S. I., F. R. Greten and M. Karin (2010). "Immunity, inflammation, and cancer." Cell **140**(6): 883-899.

Han, M. S., D. Y. Jung, C. Morel, S. A. Lakhani, J. K. Kim, R. A. Flavell and R. J. Davis (2013). "JNK expression by macrophages promotes obesity-induced insulin resistance and inflammation." Science **339**(6116): 218-222.

Jha, K. N., I. A. Shumilin, L. C. Digilio, O. Chertihin, H. Zheng, G. Schmitz, P. E. Visconti, C. J. Flickinger, W. Minor and J. C. Herr (2008). "Biochemical and structural characterization of apolipoprotein A-I binding protein, a novel phosphoprotein with a potential role in sperm capacitation." Endocrinology **149**(5): 2108-2120.

Kremer, L. S., K. Danhauser, D. Herebian, D. Petkovic Ramadza, D. Piekutowska-Abramczuk, A. Seibt, W. Muller-Felber, T. B. Haack, R. Ploski, K. Lohmeier, D. Schneider, D. Klee, D. Rokicki, E. Mayatepek, T. M. Strom, T. Meitinger, T. Klopstock, E. Pronicka, J. A. Mayr, I. Baric, F. Distelmaier and H. Prokisch (2016). "NAXE Mutations Disrupt the Cellular NAD(P)HX Repair System and Cause a Lethal Neurometabolic Disorder of Early Childhood." Am J Hum Genet **99**(4): 894-902.

Lawrence, T. and G. Natoli (2011). "Transcriptional regulation of macrophage polarization: enabling diversity with identity." Nat Rev Immunol **11**(11): 750-761.

Mao, R., S. Meng, Q. Gu, R. Araujo-Gutierrez, S. Kumar, Q. Yan, F. Almazan, K. A. Youker, Y. Fu, H. J. Pownall, J. P. Cooke, Y. I. Miller and L. Fang (2017). "AIBP Limits Angiogenesis Through gamma-Secretase-Mediated Upregulation of Notch Signaling." Circ Res.

Marbaix, A. Y., G. Noel, A. M. Detroux, D. Vertommen, E. Van Schaftingen and C. L. Linster (2011). "Extremely conserved ATP- or ADP-dependent enzymatic system for nicotinamide nucleotide repair." J Biol Chem **286**(48): 41246-41252.

Marbaix, A. Y., D. Tyteca, T. D. Niehaus, A. D. Hanson, C. L. Linster and E. Van Schaftingen (2014). "Occurrence and subcellular distribution of the NADPHX repair system in mammals." Biochem J **460**(1): 49-58.

Martinez, F. O., S. Gordon, M. Locati and A. Mantovani (2006). "Transcriptional profiling of the human monocyte-to-macrophage differentiation and polarization: new molecules and patterns of gene expression." J Immunol **177**(10): 7303-7311.

Martinez, F. O., A. Sica, A. Mantovani and M. Locati (2008). "Macrophage activation and polarization." Front Biosci **13**: 453-461.

McNelis, J. C. and J. M. Olefsky (2014). "Macrophages, immunity, and metabolic disease." Immunity **41**(1): 36-48.

Moore, K. J., F. J. Sheedy and E. A. Fisher (2013). "Macrophages in atherosclerosis: a dynamic balance." Nat Rev Immunol **13**(10): 709-721.

Noy, R. and J. W. Pollard (2014). "Tumor-associated macrophages: from mechanisms to therapy." Immunity **41**(1): 49-61.

Odegaard, J. I. and A. Chawla (2013). "Pleiotropic actions of insulin resistance and inflammation in metabolic homeostasis." Science **339**(6116): 172-177.

Oh, D. Y., H. Morinaga, S. Talukdar, E. J. Bae and J. M. Olefsky (2012). "Increased macrophage migration into adipose tissue in obese mice." Diabetes **61**(2): 346-354.

Osborn, O. and J. M. Olefsky (2012). "The cellular and signaling networks linking the immune system and metabolism in disease." Nat Med **18**(3): 363-374.

Park, E. J., J. H. Lee, G. Y. Yu, G. He, S. R. Ali, R. G. Holzer, C. H. Osterreicher, H. Takahashi and M. Karin (2010). "Dietary and genetic obesity promote liver inflammation and tumorigenesis by enhancing IL-6 and TNF expression." Cell **140**(2): 197-208.

Patel, H. H. and P. A. Insel (2009). "Lipid rafts and caveolae and their role in compartmentation of redox signaling." Antioxid Redox Signal **11**(6): 1357-1372.

Plociennikowska, A., A. Hromada-Judycka, K. Borzecka and K. Kwiatkowska (2015). "Co-operation of TLR4 and raft proteins in LPS-induced pro-inflammatory signaling." Cell Mol Life Sci **72**(3): 557-581.

Rao, R., B. Logan, K. Forrest, T. L. Roszman and J. Goebel (2004). "Lipid rafts in cytokine signaling." Cytokine Growth Factor Rev **15**(2-3): 103-110.

Ritter, M., C. Buechler, A. Boettcher, S. Barlage, A. Schmitz-Madry, E. Orso, S. M. Bared, G. Schmiedeknecht, C. H. Baehr, G. Fricker and G. Schmitz (2002). "Cloning and characterization of a novel apolipoprotein A-I binding protein, AI-BP, secreted by cells of the kidney proximal tubules in response to HDL or ApoA-I." Genomics **79**(5): 693-702.

Rudolph, C., A. Sigruener, A. Hartmann, E. Orso, M. Bals-Pratsch, W. Gronwald, B. Seifert, H. R. Kalbitzer, I. Verdorfer, C. M. Luetjens, O. Ortmann, S. R. Bornstein and G. Schmitz (2007). "ApoA-I-binding protein (AI-BP) and its homologues hYjeF_N2 and hYjeF_N3 comprise the YjeF_N domain protein family in humans with a role in spermiogenesis and oogenesis." Horm Metab Res **39**(5): 322-335.

Shumilin, I. A., M. Cymborowski, O. Chertihin, K. N. Jha, J. C. Herr, S. A. Lesley, A. Joachimiak and W. Minor (2012). "Identification of unknown protein function using metabolite cocktail screening." Structure **20**(10): 1715-1725.

Tall, A. R. and L. Yvan-Charvet (2015). "Cholesterol, inflammation and innate immunity." Nat Rev Immunol **15**(2): 104-116.

Triantafilou, M., K. Miyake, D. T. Golenbock and K. Triantafilou (2002). "Mediators of innate immune recognition of bacteria concentrate in lipid rafts and facilitate lipopolysaccharide-induced cell activation." J Cell Sci **115**(Pt 12): 2603-2611.

Zhang, B., C. Zhao, K. X. Luo, G. Q. Yan, J. Yao, Y. Y. Wang, H. J. Lu, H. Z. Fan and P. Y. Yang (2010). "New lysine-acetylated proteins screened by immunoaffinity and liquid chromatography-mass spectrometry." Science China-Chemistry **53**(1): 238-244.

Zhang, M., L. Li, W. Xie, J. F. Wu, F. Yao, Y. L. Tan, X. D. Xia, X. Y. Liu, D. Liu, G. Lan, M. Y. Zeng, D. Gong, H. P. Cheng, C. Huang, Z. W. Zhao, X. L. Zheng and C. K. Tang (2016). "Apolipoprotein A-1 binding protein promotes macrophage cholesterol efflux by facilitating apolipoprotein A-1 binding to ABCA1 and preventing ABCA1 degradation." Atherosclerosis **248**: 149-159.

CHAPTER 1

# AIBP Protects Against Metabolic Abnormalities and Atherosclerosis

Dina A. Schneider[1], Soo-Ho Choi[1], Colin Agatisa-Boyle[1], Laurence Zhu[3], Jungsu Kim[1], Jennifer Pattison[1], Dorothy D. Sears[1, 2], Philip L.S.M. Gordts[1], Longhou Fang[3], Yury I. Miller[1]*

Departments of [1]Medicine and [2]Family Medicine and Public Health, University of California, San Diego, 9500 Gilman Drive, La Jolla, CA 92093; [3]Center for Cardiovascular Regeneration, Department of Cardiovascular Sciences, Houston Methodist Research Institute, 6670 Bertner Avenue, Houston, TX 77030

First published in The Journal of Lipid Research March 20, 2018

**Abstract**

Apolipoprotein A-I Binding Protein (AIBP) has been shown to augment cholesterol efflux from endothelial cells and macrophages. In zebrafish and mice, AIBP-mediated regulation of cholesterol levels in the plasma membrane of endothelial cells controls angiogenesis. The goal of this work was to evaluate metabolic changes and atherosclerosis in AIBP loss-of-function and gain-of-function animal studies. Here we show that *Apoa1bp*$^{-/-}$*Ldlr*$^{-/-}$ mice fed a high-cholesterol, high-fat diet had exacerbated weight gain, liver steatosis, glucose intolerance, hypercholesterolemia and hypertriglyceridemia, and larger atherosclerotic lesions compared to *Ldlr*$^{-/-}$ mice. Feeding *Apoa1bp*$^{-/-}$*Ldlr*$^{-/-}$ mice a high-cholesterol, normal-fat diet did not result in significant differences in lipid levels or size of atherosclerotic lesions from *Ldlr*$^{-/-}$ mice. Conversely, adeno-associated virus-mediated overexpression of AIBP reduced hyperlipidemia and atherosclerosis in high-cholesterol, high-fat diet-fed *Ldlr*$^{-/-}$ mice. Injections of recombinant AIBP reduced aortic inflammation in *Ldlr*$^{-/-}$ mice fed a short high-cholesterol, high-fat diet. Conditional overexpression of AIBP in zebrafish also reduced diet-induced vascular lipid accumulation. In experiments with isolated macrophages, AIBP facilitated cholesterol efflux to

HDL, reduced lipid rafts content, and inhibited inflammatory responses to LPS. Our data demonstrate that AIBP confers protection against diet-induced metabolic abnormalities and atherosclerosis.

## Introduction

Cardiovascular disease (CVD) is a leading cause of morbidity and mortality in the United States, accounting for approximately one-third of all US deaths (Go, Mozaffarian et al. 2014). Therapy to reduce low-density lipoprotein cholesterol (LDL-C) has led to remarkable improvement in clinical outcomes, decreasing the incidence of acute cardiovascular events by 25-35% (Baigent, Keech et al. 2005, Steinberg, Glass et al. 2008). Statins, ezetimibe, and recently apoB antisense and PCSK9 monoclonal antibodies all target plasma LDL-C as a major atherogenic factor. However, improving the other arc of cholesterol homeostasis – reverse cholesterol transport and atheroprotective high-density lipoprotein (HDL) – has proven to be a challenging task. Results of clinical trials of CETP inhibitors put in doubt the efficacy of simply raising HDL-C levels as an ultimate therapeutic goal (Tall and Rader 2018). Although HDL-C clearly correlates with atheroprotection in epidemiology studies, the current consensus in the cardiovascular field underscores the added importance of improving the functionality of HDL (Fisher, Feig et al. 2012, Heinecke 2012, Larach, deGoma et al. 2012, Rosenson, Brewer et al. 2012). However, *in vivo* mechanisms regulating HDL function are not sufficiently understood.

Our recent work and the work of others have highlighted Apolipoprotein A-I Binding Protein (AIBP), which augments cholesterol efflux from endothelial cells (Fang, Choi et al. 2013, Mao, Meng et al. 2017) and macrophages (Zhang, Li et al. 2016) to HDL. AIBP is a secreted protein discovered in a screen of proteins that physically associate with apoA-I (Ritter,

Buechler et al. 2002). Human *APOA1BP* mRNA encoding the AIBP protein is ubiquitously expressed, with the highest expression in kidney, heart, liver, thyroid gland, adrenal gland and testis (Ritter, Buechler et al. 2002). AIBP protein is found in cerebrospinal fluid and urine, and in plasma of patients with sepsis (Ritter, Buechler et al. 2002). The human *APOA1BP* gene is located at 1q21.2-1q22 on chromosome 1, which corresponds to the 1q21-q23 locus for familial combined hyperlipidemia, a common multifactorial and heterogeneous dyslipidemia predisposing to premature coronary artery disease (Bodnar, Chatterjee et al. 2002). Yet, there are no studies directly linking AIBP polymorphism with dyslipidemia or risk of CVD.

AIBP does not bind cholesterol nor induce cholesterol efflux in the absence of HDL or apoA-I, but it does increase the turnover of HDL and thus accelerates cholesterol efflux (Fang, Choi et al. 2013). The goal of this work was to evaluate metabolic changes and atherosclerosis in AIBP loss-of-function and gain-of-function animal studies. We report that AIBP deficiency exacerbates weight gain, hyperlipidemia and atherosclerosis, while overexpression of AIBP is protective against vascular lipid accumulation, atherosclerosis, and metabolic abnormalities.

## Methods

### *Animals and diets*

All animal experiments were conducted according to protocols approved by the Institutional Animal Care and Use Committee of the University of California, San Diego. Mice were housed up to 5 per standard cage at room temperature and maintained on a 12:12 hour light:dark cycle, with lights on at 07:00. Both food and water were available ad libitum. Wild type C57BL/6 and *Ldlr*$^{-/-}$ mice were initially purchased from Jackson Lab (Bar Harbor, ME) and bred in-house for experiments. *Apoa1bp*$^{-/-}$ mice on a C57BL/6 background were generated in our group as

previously described (Mao, Meng et al. 2017) and cross-bred with *Ldlr*$^{-/-}$ mice. *Apoa1bp*$^{-/-}$*Ldlr*$^{-/-}$ mice develop and breed normally. For metabolic studies, mice on a C57BL/6 background were fed a high-fat diet (Research Diets D12451; Supplemental Table S1) containing 45% kcal from fat, starting at age 10 weeks. For metabolic and atherosclerosis studies, mice on an *Ldlr*$^{-/-}$ background were fed either a Western Diet (Teklad TD.96121; Supplemental Table S2) containing 42% kcal from fat (21% milkfat) and 1.25% cholesterol, or a high-cholesterol, normal-fat diet (Teklad TD.97131; Supplemental Table S3) containing 1% cholesterol, starting at age 8 weeks.

Adult zebrafish were maintained at 28°C on a 14-hour-light/10-hour-dark cycle as previously described (Westerfield 2007) and fed brine shrimp twice a day. Zebrafish larvae were fed Golden Pearls (Brine Shrimp Direct, Ogden, UT) twice a day, starting from 5 dpf. The transgenic *hsp70:apoa1bp-2A-mRFP* zebrafish was generated using constructs and methods previously described (Fang, Green et al. 2011, Kim, Lee et al. 2011, Fang, Choi et al. 2013). The self-cleavage 2A peptide allows for expression of two separate proteins in the same tissue, with mRFP serving as an indicator of successful protein expression. Transgene expression was initiated by single or repeated heat shocks (transferring zebrafish for 1 hour into water warmed to 37°C) and detected via mRFP fluorescence. Expression of the zebrafish Apoa1bp protein was confirmed in western blot with a guinea pig polyclonal anti-zebrafish Apoa1bp antibody (Fang, Choi et al. 2013). For vascular lipid deposit experiments, Golden Pearls supplemented with 4% (w/w) cholesterol and 1 μg/g of TopFluor Cholesterol (Avanti Polar Lipids), were fed to zebrafish from 5 to 15 dpf as described (Fang, Green et al. 2011). Zebrafish were imaged using a Nikon A1 confocal microscope and images were analyzed as described (Fang, Green et al. 2011).

*Cohort sizes and blinding*

Cohort sizes for experiments involving *Apoa1bp*$^{-/-}$ mice, which were considered the major goal of the study, were calculated based on an assumption that the difference between means will be 1.3-2.0 fold, with standard deviations of 10-50% of mean, depending on experiment; 80% power, and $p<0.05$. Animals were assigned to respective groups randomly within genotype. Individuals performing atherosclerosis analysis were not informed of genetic background or hypothesis.

*Glucose, insulin, and glucose tolerance test*

Glucose tolerance test was performed at 8 weeks of diet feeding and 18 weeks of age. Mice on the C57BL/6 background were fasted four hours prior to testing. Glucose was administered to mice at a dose of 1g/kg of body weight via IP injection of 25% dextrose in sterile saline (VetOne). Blood was collected from tail at time 0, 10, 30, 60, 90, and 120 minutes and blood glucose was measured on a OneTouch Ultra glucose monitor. Additional blood was collected into heparinized capillary tubes at times 0 and 10 minutes for measurement of plasma insulin via ELISA (Alpco; catalog #80-INSMSH-E01). In cohorts of mice on the Ldlr$^{-/-}$ background, plasma was isolated from terminal blood, and plasma glucose levels were measured using a kit from Crystal Chem (catalog #81692) and insulin levels using an ultrasensitive insulin ELISA (Alpco; catalog #80-INSMSU-E01).

*Lipids and lipoprotein profile*

Blood was collected from mice into EDTA tubes upon sacrifice and plasma was collected following centrifugation. Lipoprotein profiles were determined by pooling plasma from each

genotype and quantifying cholesterol content of each fraction via FPLC with a Superose 6 column.

*Atherosclerosis Studies*

Atherosclerosis was assessed as previously described (Tsimikas, Miyanohara et al. 2011). Briefly, *En face* atherosclerosis was quantified via computer-assisted image analysis (ImagePro) of Sudan-stained whole aorta. Aortic root atherosclerosis was quantified by cutting cross-sections starting from the aortic origin until the last leaflet. Sections were stained with a modified Van Gieson stain and lesion area was quantified via computer-assisted image analysis (ImagePro).

*Cells*

RAW264.7 cells were cultured in DMEM (Cellgro) supplemented with 10% heat-inactivated FBS (Omega Scientific) and 50 μg/ml gentamicin (Omega Scientific).

*Western blot*

Cell and tissue lysates were subjected to gel electrophoresis and immunoblot as described (Choi, Wiesner et al. 2012). Antibodies were purchased from Cell Signaling Technology: p65 (catalog #4767), phospho-p65 (catalog #3033), ERK1/2 (catalog #4695), phospho-ERK1/2 (catalog #9101), and GAPDH (catalog #2118).

*Quantitative PCR*

Total RNA was isolated using Nucleospin RNA columns (Clontech). Isolated RNA was reverse transcribed using RNA to cDNA EcoDry (Clontech) following the manufacturer's protocol. Quantitative PCR was performed using KAPA SYBR FAST Universal qPCR kit (KAPA Biosystems, KK4602), with primers ordered from Integrated DNA Technologies (IDT), and a Rotor Gene Q thermocycler (Qiagen). Primer sequences are listed in Supplemental Table S4.

*Recombinant AIBP*

AIBP was produced in a baculovirus/insect cell system to allow for post-translational modification and to ensure endotoxin-free preparation. Human AIBP was cloned into a pAcHLT-C vector behind the polyhedrin promoter. The vector contains an N-terminal His-tag to enable purification and detection. Insect Sf9 cells were transfected with BD BaculoGold Baculovirus DNA and the AIBP vector. After 4-5 days, the supernatant was collected to afford a baculovirus stock. Fresh Sf9 cells were infected with the AIBP-producing baculovirus, cell pellets were collected after 3 days, lysed, sonicated, cleared by centrifugation, and the supernatants loaded onto a Ni-NTA agarose column and eluted with imidazole. Protein was dialyzed against PBS, and concentration measured. Aliquots were stored at -80$^{o}$C.

*LPS/Kdo2-LipidA*

In vitro experiments were conducted with Kdo2-LipidA (Avanti Polar Lipids), a well-characterized active component of LPS and a highly specific TLR4 agonist (Raetz, Garrett et al. 2006). In text and figure legends, we refer to Kdo2-LipidA as LPS.

*AAV2-AIBP*

Mouse AIBP (25-283 aa) was fused with fibronectin secretion sequence (FIB) at the N-terminus and 6X-His at the C-terminus (FIB-AIBP-His). FIB-AIBP-His was cloned into the pAAV-MCS vector (Agilent Technologies). All clones were sequenced to confirm the presence of the insert. AAV-293 cells (Agilent Technologies) were transfected with 20 μg of each pAAV-FIB-AIBP-His, pAAV2 (Agilent Technologies), and pHelper DNA (Agilent Technologies) following the routine calcium phosphate-based protocol (Agilent Technologies). Subsequent steps of virus harvest, purification and storage were according to published protocols (Huang, Hartley et al. 2013). Viral DNA was extracted from purified virus and the number of gene copies (gc) was determined using qPCR with primers for the inverted terminal repeats (Takara Bio Inc). Testing the FIB-AIBP-His plasmid and the AAV2-FIB-AIBP-His, we found that infected HEK 293 cells expressed AIBP of the correct molecular mass, recognized by anti-His (ThermoFisher, catalog #MA1-21315). For AAV2-mediated AIBP expression, *Ldlr*$^{-/-}$ mice were intravenously injected with empty virus or AAV2-AIBP at $1x10^{12}$ gc/mouse. At 3 weeks post-injection, mice were fed Western diet (Teklad TD.96121) for additional 16 weeks. Testing for the expression of FIB-AIBP-His, liver was homogenized in RIPA buffer and lysates were analyzed in western blot.

*White Adipose Tissue FACS*

Flow cytometry of WAT was performed as previously described (Sears, Miles et al. 2009). In brief, mice were sacrificed, and tissue was perfused with PBS. White adipose tissue was minced in 5% BSA DPBS and centrifuged to remove erythrocytes and free leukocytes. Tissue was dissociated using collagenase (Sigma C6885), filtered, and separated from adipocytes via centrifugation. The stromal vascular fraction was used for FACS analysis. Antibodies used were

CD11b-FITC (BD 553310), F4/80-APC (Ab Serotec MCA497APC), and CD11c-PE (BD 553802).

*Cholesterol Efflux and Lipid Raft Assays*

A cholesterol efflux assay was performed as described (O'Connell, Denis et al. 2004, Whetzel, Sturek et al. 2010), with modifications. In brief, RAW264.7 cells were loaded with 2 µCi/mL [$^3$H]-cholesterol (American Radiolabeled Chemicals), and cholesterol efflux was initiated by the addition of efflux medium containing 25 µg/mL HDL, in the presence or absence of 0.2 µg/mL recombinant AIBP, for 4 hours. Background, nonspecific release of [$^3$H]-cholesterol was measured in the absence of HDL. After incubation, the medium was collected and counted in a liquid scintillation counter LS 6500 (Beckman Coulter). The cells were extracted with 2-propanol, and the lipid extract was added to ScintiVerse BD Cocktail (Fisher) and counted. Cholesterol efflux was expressed as a percentage of [$^3$H] counts in the medium compared to combined [$^3$H] counts in the cells and the medium. In these experiments, to replicate *in vivo* conditions, cells were not treated with an LXR agonist or ACAT inhibitor.

For lipid raft measurements, RAW264.7 macrophages were incubated with FITC-conjugated cholera toxin B (Sigma) for 1 hour on ice. Cells were washed two times with a FACS buffer, fixed with 3.7% formaldehyde for 15 min on ice, washed three times with a FACS buffer, and analyzed using a FACSCanto II (BD Biosciences) flow cytometer.

*Statistical Analyses*

Results were analyzed using Student's t-test (for differences between 2 groups), one-way ANOVA (for multiple groups), or two-way ANOVA with the Bonferroni post hoc test (for

multiple groups time course experiments), using GraphPad Prism. Differences between groups with $p<0.05$ were considered statistically significant. Values were excluded if determined to be a significant outlier via the extreme studentized deviate test.

## Results

*Metabolic abnormalities in AIBP mice*

Systemic *Apoa1bp* knockout mice have been developed in our lab as described (Mao, Meng et al. 2017). C57BL/6 and *Apoa1bp*$^{-/-}$ mice were fed a high-fat, normal-cholesterol diet (HFD) for 10 weeks starting from the age of 10 weeks. Despite having similar weights prior to diet feeding, *Apoa1bp*$^{-/-}$ mice were significantly heavier than their wild type counterparts following the diet, despite consuming equivalent amounts of food (Fig. 1a and b). *Apoa1bp*$^{-/-}$ mice also exhibited impaired glucose clearance and increased circulating plasma insulin levels when subjected to a glucose tolerance test (Fig. 1c-e). Flow cytometry analysis of the white adipose tissue (WAT) stromal vascular fraction revealed that epididymal WAT from *Apoa1bp*$^{-/-}$ mice contained a greater proportion of F4/80+CD11b+CD11c+ pro-inflammatory macrophages (Fig. 1f). Overall, *Apoa1bp*$^{-/-}$ mice exhibited more hallmarks of metabolic disease than their wild type counterparts when fed a HFD.

Similar to HFD-fed *Apoa1bp*$^{-/-}$ mice, *Apoa1bp*$^{-/-}$*Ldlr*$^{-/-}$ mice fed a Western diet (high-fat, high-cholesterol) for 12 weeks became significantly heavier than *Ldlr*$^{-/-}$ mice (Fig. 2a). The livers of *Apoa1bp*$^{-/-}$*Ldlr*$^{-/-}$ mice had increased cholesterol and triglyceride content (Fig. 2b and c). Liver expression of TNFα mRNA was increased nearly 3-fold in *Apoa1bp*$^{-/-}$*Ldlr*$^{-/-}$ mice, suggesting increased liver inflammation (Fig. 2d). Plasma levels of glucose and insulin trended higher in terminal blood of non-fasted *Apoa1bp*$^{-/-}$*Ldlr*$^{-/-}$ mice (Supplemental Fig. S1a and b).

*AIBP deficiency results in exacerbated hyperlipidemia and atherosclerosis*

*Apoa1bp*$^{-/-}$*Ldlr*$^{-/-}$ mice fed a Western diet had higher plasma cholesterol and triglyceride levels, primarily due to elevated VLDL and LDL, as compared to *Ldlr*$^{-/-}$ mice (Fig. 3a-d). Importantly, atherosclerotic lesions in the aortic root were significantly larger in *Apoa1bp*$^{-/-}$*Ldlr*$^{-/-}$ mice compared to *Ldlr*$^{-/-}$ mice (Fig. 3e-g). Overall, mice lacking AIBP had significantly increased weight gain, lipid levels in both plasma and liver tissue, and atherosclerosis when fed a high-fat, high-cholesterol diet. However, feeding *Apoa1bp*$^{-/-}$*Ldlr*$^{-/-}$ mice a diet enriched in cholesterol (1%) but with normal fat content, did not result in significant differences in weight, plasma cholesterol, triglycerides or glucose levels, or atherosclerosis when compared to *Ldlr*$^{-/-}$ mice (Fig. 4 and Supplemental Fig. S1c). Plasma insulin levels in *Apoa1bp*$^{-/-}$*Ldlr*$^{-/-}$ mice were higher than in *Ldlr*$^{-/-}$ mice, but absolute numbers remained low (Supplemental Fig. S1d). These results suggest the importance of AIBP-mediated metabolic changes in the development of atherosclerosis in the context of high-fat, high-cholesterol diets.

*AAV-mediated expression of AIBP reduces weight gain, hyperlipidemia, and atherosclerosis*

Next, we tested if sustained overexpression of mouse AIBP can reduce atherosclerosis. We generated an AAV2 with the FIB-AIBP-His construct. The fibronectin signal peptide (FIB) was inserted to ensure secretion of His-tagged mouse AIBP. Five-week-old *Ldlr*$^{-/-}$ mice were infected with AAV2-AIBP or the empty AAV2 (control) and, starting at 8 weeks of age, were fed a Western diet for 16 weeks. At the time of sacrifice, livers were collected to confirm AIBP-His protein expression (Supplemental Fig. S2); however, AIBP-His was not detectable in plasma. Both the control cohort and AAV2-AIBP cohort had similar weights prior to the start of

the diet, but the mice overexpressing AIBP were significantly protected against diet-induced weight gain (Fig. 5a). Liver triglyceride levels were significantly lower and cholesterol levels trended lower in mice infected with AAV2-AIBP compared to the mice infected with the empty AAV2 (Fig. 5b and c). Plasma cholesterol levels had a trend towards reduction (Fig. 5 d and e), and plasma triglycerides were significantly decreased (Fig. 5f and g). Importantly, there was a significant decrease in *en face* lesions (Fig. 5h), as well as a trend of reduced aortic root atherosclerosis in the AAV2-AIBP mice (Fig. 5i and j). Taken together, these data show protection against weight gain, plasma lipid increases, and atherosclerosis by AAV-delivered AIBP.

*Transgenic AIBP expression in zebrafish reduces diet-induced vascular lipid accumulation*

We have previously described a hyperlipidemic zebrafish model in which vascular accumulation of lipid deposits was observed in live animals 10-14 days after initiation of high-cholesterol feeding (Stoletov, Fang et al. 2009, Fang, Green et al. 2011). To investigate whether AIBP can reduce lipid accumulation in the vasculature, we generated a transgenic zebrafish line in which expression of the *apoa1bp-2A-mRFP* construct is controlled by the *hsp70* heat shock promoter (Fig. 6a). Following protein expression, self-cleavage of the translated 2A peptide (Kim, Lee et al. 2011) releases untagged, zebrafish Apoa1bp and mRFP, the latter serving as a reporter for Apoa1bp expression. Heat shock-induced expression of the Apoa1bp protein was confirmed in western blot (Fig. 6b). When zebrafish were fed a high-cholesterol diet (HCD) supplemented with fluorescently-labeled cholesterol for 10 days, vascular lipid deposits increased significantly (Fig. 6c and d). Our previous work has shown that heat shock itself does not affect diet-induced vascular lipid accumulation (Fang, Green et al. 2011). However, heat

shock-induced overexpression of Apoa1bp prevented the HCD-induced increase in vascular lipid deposition (Fig. 6c and d), independently supporting the hypothesis that AIBP overexpression is atheroprotective.

*Recombinant AIBP inhibits inflammatory responses by macrophages*

Because AIBP was shown to augment HDL function (Fang, Choi et al. 2013, Mao, Meng et al. 2017) and AIBP deficiency resulted in a higher liver expression of *Tnfa* (Fig. 2d), we hypothesized that AIBP reduces inflammatory responses by macrophages. In cell culture experiments, recombinant AIBP significantly increased cholesterol efflux from RAW264.7 macrophages (Fig. 7a) and reduced lipid raft content as assessed by FACS analysis of Cholera Toxin B (CTB) binding to cells (Fig. 7b). To test whether AIBP inhibits inflammatory signaling, RAW264.7 macrophages were stimulated with lipopolysaccharide (LPS), in the presence of AIBP or BSA control. LPS-induced phosphorylation of p65 and ERK1/2 in macrophages was significantly reduced in AIBP-treated cells (Fig. 7c-e). In addition, recombinant AIBP significantly reduced gene expression of inflammatory cytokines in macrophages that were stimulated with LPS+IFNγ, a common inflammatory, M1-like polarization signal (Fig. 8a-f).

We next tested if injections of recombinant AIBP can reduce vascular inflammation in mice. Hyperlipidemic *Ldlr*$^{-/-}$ mice that had been fed a Western Diet for 4 weeks were injected three times during the final week of feeding with PBS control, AIBP or heat-inactivated AIBP. Injections did not affect mouse weight or plasma lipids (Fig. 9a-c). Aortas of these mice were used for total RNA isolation and gene expression analysis via qPCR. While heat-inactivated AIBP had no effect, non-denatured AIBP injection significantly reduced transcript levels of the inflammatory cytokines IL-6, IL-1β, and CCL2 compared to PBS treated mice (Fig. 9d).

**Discussion**

In this study, using loss-of-function and gain-of-function animal models, we explored the role of AIBP in metabolism and atherosclerosis. We found that *Apoa1bp*$^{-/-}$*Ldlr*$^{-/-}$ mice fed a Western diet had exacerbated liver steatosis, hyperlipidemia and atherosclerosis. Conversely, AIBP gain-of-function resulted in reduced vascular lipid accumulation in zebrafish and in reduced aortic inflammation, hyperlipidemia and atherosclerosis in mice. These results suggest that AIBP restricts diet-induced metabolic abnormalities and is atheroprotective.

The results of our experiments demonstrate that the AIBP control of diet-induced metabolic abnormalities is an important factor in atheroprotection. Intravenous injections of recombinant AIBP into mice reduced hyperlipidemia-induced inflammation in the aorta, which is considered one of the earliest sites of diet-induced insulin resistance, preceding both liver and white adipose tissue (Kim, Pham et al. 2008). A sustained gain-of-function of AIBP, delivered via the AAV2-AIBP, resulted in protection against weight gain, hypertriglyceridemia and atherosclerosis. Most tellingly, the AIBP knockout did not exacerbate atherosclerosis in the mice fed a normal-fat, high-cholesterol diet, which does not elicit a metabolic response in *Ldlr*$^{-/-}$ mice (Hartvigsen, Binder et al. 2007). However, when fed a high-fat, normal-cholesterol diet (HFD), *Apoa1bp*$^{-/-}$ mice gained more weight and were more glucose intolerant than C57BL/6 mice, despite consuming equal quantities of food. Similarly, *Apoa1bp*$^{-/-}$*Ldlr*$^{-/-}$ mice fed a high-fat, high-cholesterol diet, gained more weight and developed more severe hepatic steatosis, compared to *Ldlr*$^{-/-}$ mice. The resulting exacerbation of hypertriglyceridemia and hypercholesterolemia led to more atherosclerosis in high-fat, high-cholesterol diet-fed *Apoa1bp*$^{-/-}$*Ldlr*$^{-/-}$ mice.

Interestingly, a recent study of mice with reduced expression of ABCA1 in adipocytes and macrophages (Chung, Sawyer et al. 2011) demonstrates that they share a similar phenotype of weight gain, increased plasma triglycerides, increased liver cholesterol and triglyceride levels, as well as the impaired glucose tolerance (de Haan, Bhattacharjee et al. 2014), found in the AIBP knockout mice. Increased fat mass and insulin resistance are linked to an increase in VLDL synthesis and a reduction in triglyceride-rich lipoprotein uptake (Laatsch, Merkel et al. 2009, Choi and Ginsberg 2011), both of which may contribute to the high VLDL plasma content in *Apoa1bp*$^{-/-}$*Ldlr*$^{-/-}$ mice. With greater exhibition of metabolic abnormalities, inflammatory macrophage signaling favored, and increased plasma cholesterol, it is expected that *Apoa1bp*$^{-/-}$ *Ldlr*$^{-/-}$ mice have significantly increased prevalence of aortic root atherosclerosis.

Systemic low-grade inflammation is an underlying cause of numerous pathologies, including the metabolic syndrome and atherosclerosis. A prevalent source of inflammatory cytokines are tissue macrophages, which become activated by danger-associated molecular patterns (DAMPs) arising in subjects consuming Western-type diets (Wada and Makino 2016). Receptors for many DAMPs and inflammatory cytokines, such as TLR4 and IFNGR, reside in lipid rafts, which provide an ordered microenvironment for receptor dimerization and signaling complex assembly (Lawrence and Natoli 2011, Plociennikowska, Hromada-Judycka et al. 2015). AIBP suppresses inflammatory signaling by enhancing cholesterol efflux from macrophages and thus depleting the lipid raft signaling platform. In AIBP knockout mice, the absence of AIBP results in an increase in the inflammatory milieu in the white adipose tissue and liver to propagate insulin resistance. In turn, lipids accumulate in the liver, and circulating VLDL levels increase. Excessive plasma VLDL leads to an increase in adipose triglycerides and mouse weight gain, as well as vascular lipid accumulation and atherosclerosis.

There are several limitations to our study. We considered only function of the secreted, extracellular AIBP. Several papers have been published proposing and testing intracellular functions of AIBP using *in vitro* test tube assays (Jha, Shumilin et al. 2008, Marbaix, Noël et al. 2011, Shumilin, Cymborowski et al. 2012). They suggest that intracellular AIBP may function as either an NAD(P)H-hydrate epimerase, often abbreviated as NAXE, or an ADP-ribosyltransferase, but so far, the *in vivo* significance associated with this enzymatic activity remains unclear. Yet, we cannot rule out the potential effects of intracellular AIBP on metabolic abnormalities in our mouse studies. However, we have shown ample evidence here that extracellular AIBP has an important role in regulating cholesterol efflux and lipid metabolism both *in vitro* and *in vivo* using animal models of gain-of-function of secreted or recombinant AIBP protein. Another consideration is that extracellular AIBP can have effects on multiple tissue types. Tissue-specific knockout of AIBP cannot address this issue in full, as AIBP may be secreted from an adjacent tissue. This is an important avenue for future research.

We have shown here, using a variety of animal models, that addition of AIBP is atheroprotective, while conversely the absence of AIBP is atherogenic. AIBP is highly conserved, acts, at least in part, extracellularly, and augments protective properties of HDL. Further exploration of atheroprotective properties of AIBP may help design future therapeutic interventions.

**Acknowledgements**

We would like to thank Dr. Wonkyu Ju for his help with AAV2 reagents and expertise.

I would like to acknowledge my coauthors Soo-Ho Choi, Colin Agatisa-Boyle, Laurence Zhu, Jungsu Kim, Jennifer Pattison, Dorothy D. Sears, Philip L.S.M. Gordts, Longhou Fang, and

Yury I. Miller for their contributions to Chapter 1, as well as the publishing journal The Journal of Lipid Research.

Chapter 1, in full, is a reprint of the material as it appears in The Journal of Lipid Research 2018. Schneider, Dina A.; Choi, Soo-Ho; Agatisa-Boyle, Colin; Zhu, Laurence; Kim, Jungsu; Pattison, Jennifer; Sears, Dorothy D.; Gordts, Philip L.S.M.; Fang, Longhou; Miller, Yury I., The American Society for Biochemistry and Molecular Biology, 2018. The dissertation author was the primary investigator and author of this paper.

**Sources of Funding**

This study was supported by grants HL135737, HL136275, HL088093 (Y.I.M.), HL114734 and HL132155 (L.F.) from the National Institutes of Health, 15BGIA25550111 (P.L.S.M.G.) and SDG14710028 (S.-H.C.) from the American Heart Association, and 16CVD01 form the Leducq Foundation (P.L.S.M.G.).

**Competing Financial Interests**

The authors declare no competing financial interests.

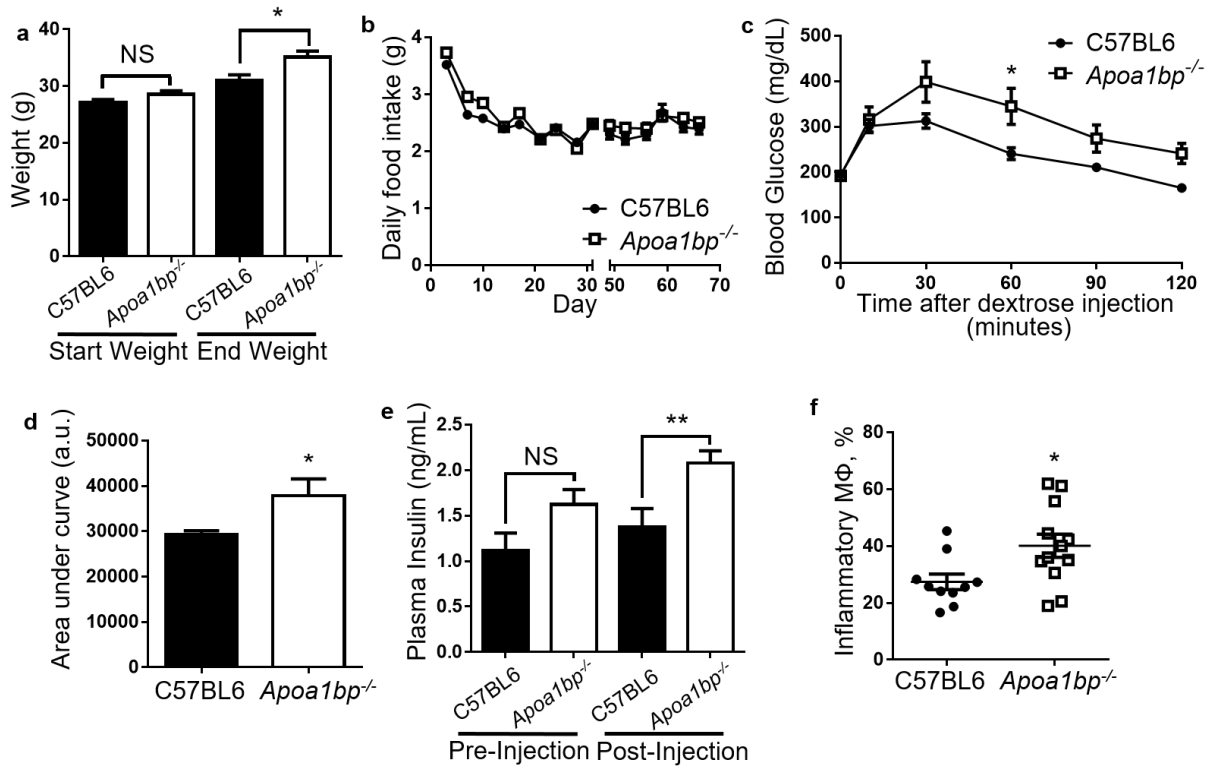


**Figure 1.1. Mice lacking AIBP exhibit metabolic abnormalities.** C57BL/6 and *Apoa1bp*$^{-/-}$ mice were fed a high-fat diet (HFD) containing 45% (kcal) fat for 10 weeks starting at age 10 weeks. **a,** Mice were weighed at start and completion of diet (Student's t-test). **b,** Food intake was measured twice a week for the duration of the 10 week feeding period, with an interruption (X-scale break) while mice were moved and housed for metabolic testing. Prior to metabolic testing, mice were group-housed and measurements given are based upon cage averages. No error bars are shown during the period for this reason. Following metabolic testing, all animals were individually housed and measurements given represent the average of all individual mice. Error bars are only shown for the singly-housed time period and are SEM. **c,** Glucose tolerance test. At week 8 of HFD feeding mice were injected with dextrose solution and blood was collected at time points shown (two-way ANOVA with Bonferroni's post-hoc test). **d,** Integrated glucose levels (area under the curve from panel c; Student's t-test). **e,** Insulin levels during glucose tolerance test at time 0 and 10 minutes (Student's t-test). **f,** Upon sacrifice at 10 weeks of feeding, white adipose tissue was harvested from mice. Cells in the isolated stromal vascular fraction were characterized by FACS analysis. Inflammatory macrophages were defined as F4/80+CD11b+CD11c+ (Student's t-test). Mean±SEM; n=10-12; **, $p<0.01$; *, $p<0.05$.

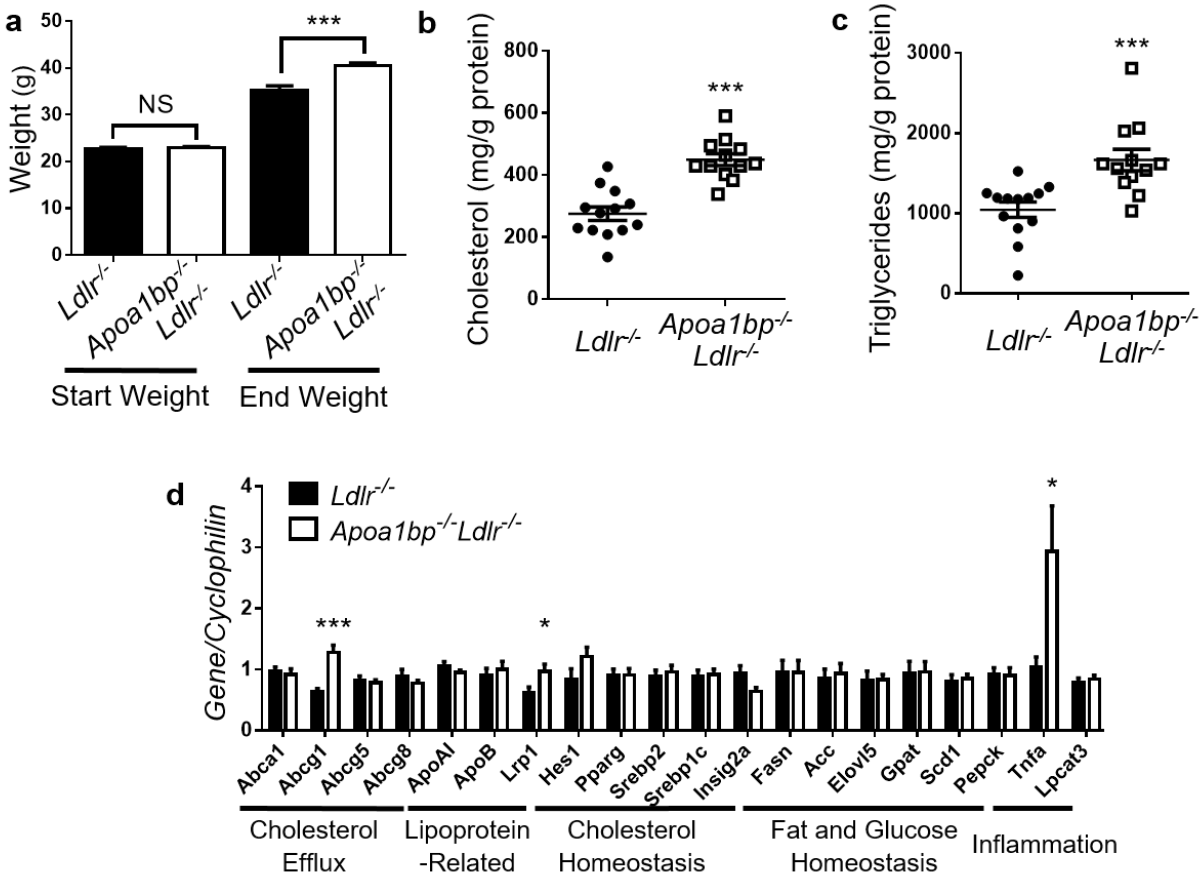


**Figure 1.2. Weight gain, liver lipid content and gene expression profile in AIBP-deficient mice fed Western diet.** *Ldlr*$^{-/-}$ and *Apoa1bp*$^{-/-}$*Ldlr*$^{-/-}$ mice were fed a Western diet containing 1.25% cholesterol and 42% kcal from fat for 12 weeks starting from age 8 weeks. **a,** Mouse weights. **b,** Cholesterol content and **c,** triglyceride content in liver. **d,** Liver gene expression. Mean±SEM; n=12-13; ***, $p<0.001$; **, $p<0.01$ ; *, $p<0.05$ (Student's t-test).

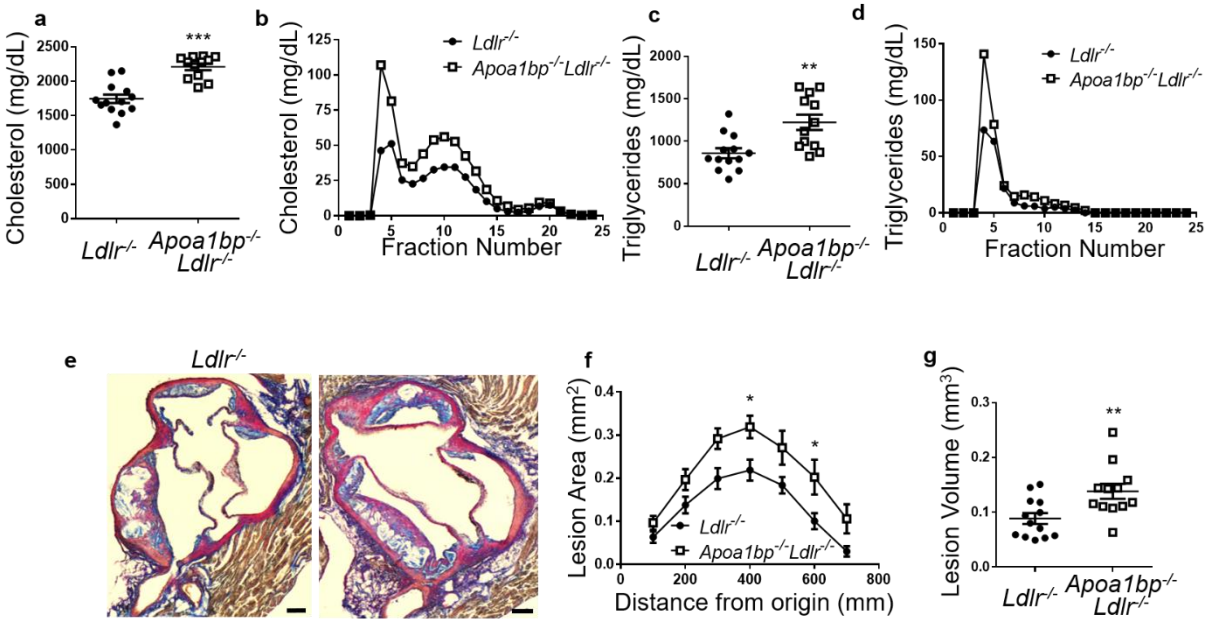


**Figure 1.3. Exacerbated hyperlipidemia and atherosclerosis in AIBP-deficient mice fed Western diet.** *Ldlr*$^{-/-}$ and *Apoa1bp*$^{-/-}$*Ldlr*$^{-/-}$ mice were fed a Western diet containing 1.25% cholesterol and 42% kcal from fat for 12 weeks starting from age 8 weeks. **a-d,** Plasma lipids at sacrifice. Total cholesterol (**a**)**,** cholesterol lipoprotein profile (**b**), total triglycerides (**c**), and triglyceride lipoprotein profile (**d**) (n=12-13, Student's t-test). **e,** Representative images of aortic root from each genotype, at 0.3 mm from aortic valve origin. Scale bar, 100 μm. **f,** Aortic root atherosclerotic lesion size as a function of distance from first leaflet appearance (n=12-13, two-way ANOVA with Bonferroni's post-hoc test). **g,** Aortic root lesion volume (area under the curve from panel f; n=12-13, Student's t-test). Mean±SEM; ***, p<0.001; **, p<0.01; *, p<0.05.

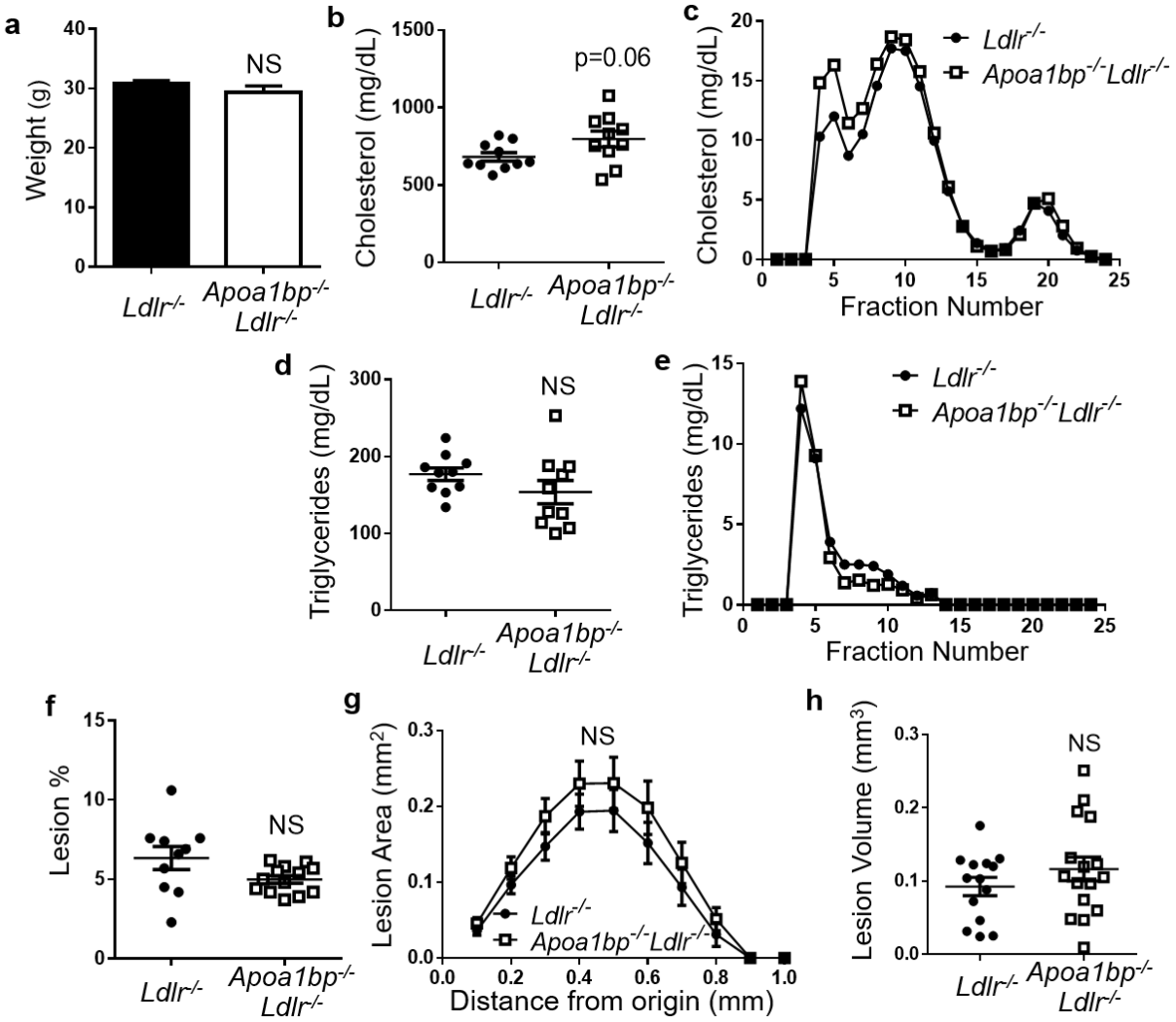


**Figure 1.4. Unchanged weight gain, hyperlipidemia and atherosclerosis in AIBP-deficient mice fed high-cholesterol, normal-fat diet.** *Ldlr*$^{-/-}$ and *Apoa1bp*$^{-/-}$*Ldlr*$^{-/-}$ mice were fed a 1% cholesterol, normal-fat diet for 16 weeks starting from age 8 weeks. **a,** Weight at the time of sacrifice (n=10; Student's t-test). **b-e,** Plasma lipids at sacrifice. Total cholesterol (**b**), cholesterol lipoprotein profile (**c**), total triglycerides (**d**), and triglyceride lipoprotein profile (**e**) (n=10, Student's t-test). **f,** *En face* atherosclerotic lesions (n=10; Student's t-test). **g,** Aortic root atherosclerotic lesion size as a function of distance from first leaflet appearance (n=16; two-way ANOVA with Bonferroni's post-hoc test). **h,** Aortic root lesion volume (area under the curve from panel g; n=16, Student's t-test). Mean±SEM; NS, not significant differences.

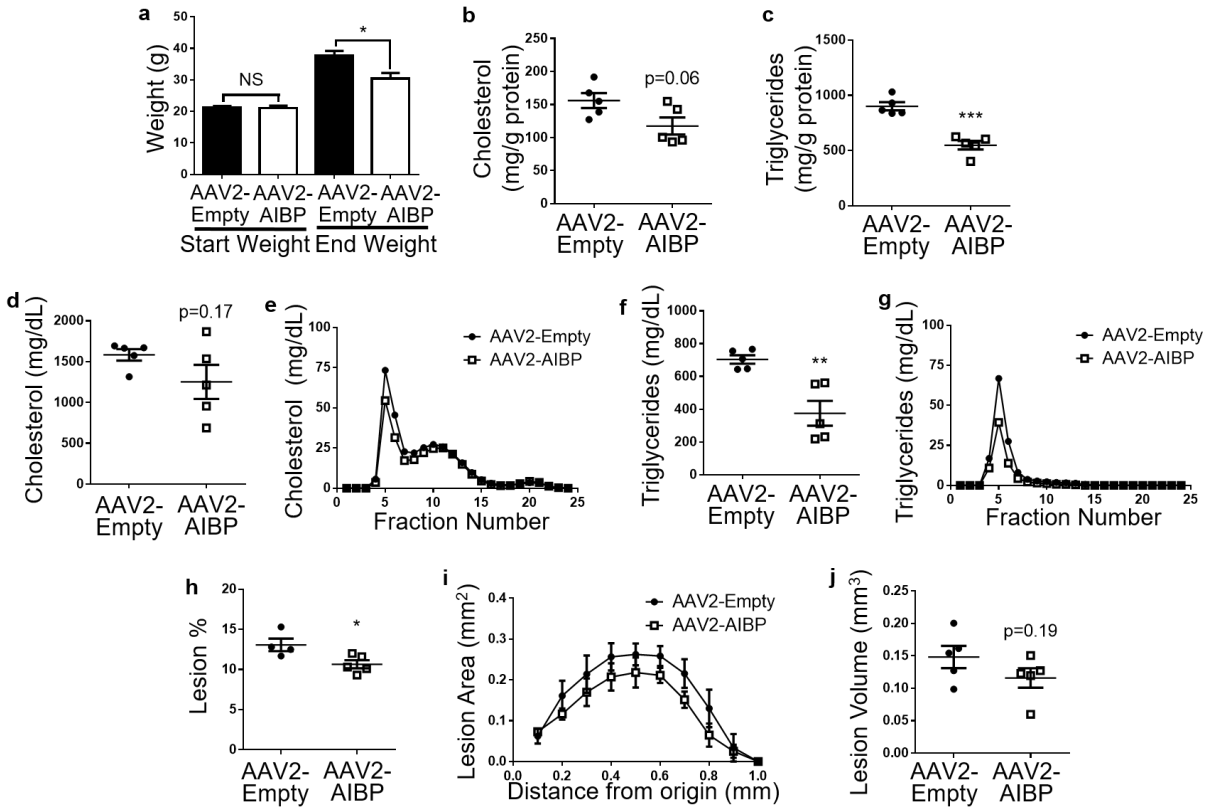


**Figure 1.5. Mice overexpressing AIBP are protected from weight gain, lipid abnormalities, and atherosclerosis.** *Ldlr*$^{-/-}$ mice were injected with either AAV2-AIBP or the empty AAV2, and fed a Western diet containing 1.25% cholesterol and 42% (kcal) fat for 16 weeks starting from age 8 weeks. **a,** Mice were weighed at start and completion of diet (Student's t-test). **b-c,** Liver total cholesterol and triglyceride levels (Student's t-test). **d-e,** Plasma total cholesterol levels (Student's t-test) and the cholesterol lipoprotein profile. **f-g,** Plasma triglyceride levels (Student's t-test) and the triglyceride lipoprotein profile. **h,** Whole aorta *en face* lesion size (Student's t-test). **i,** Aortic root atherosclerotic lesion size as a function of distance from first leaflet appearance (two-way ANOVA with Bonferroni's post-hoc test). **j,** Aortic root lesion volume (area under the curve from panel i; Student's t-test). Mean±SEM; n=5; ***, $p<0.001$; **, $p<0.01$; *, $p<0.05$.

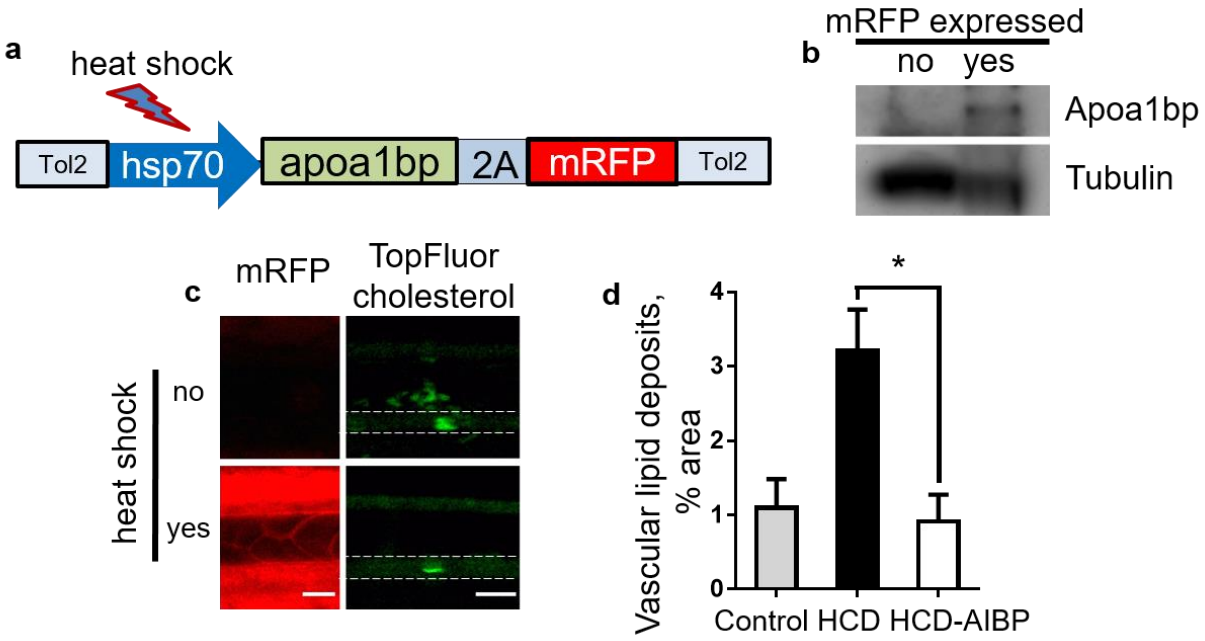


**Figure 1.6. Induced AIBP expression in zebrafish reduces diet-induced vascular lipid accumulation. a,** Construct used to make transgenic *hsp70:apoa1bp-2A-mRFP* zebrafish. **b,** Heat shock-induced Apoa1bp protein expression. Embryos were subjected for 1 hour to heat shock (37°C), at 1 dpf and again at 2 dpf. Three mRFP-negative and three mRFP-positive embryos were selected and homogenized in SDS-PAGE loading buffer. Lysates were run on SDS-PAGE, blotted and probed with anti-zebrafish Apoa1bp and tubulin antibodies. **c,** Vascular lipid accumulation. Transgenic *hsp70:apoa1bp-2A-mRFP* zebrafish were fed control or 4% cholesterol diet supplemented with TopFluor-cholesterol for 10 days, and one group was subjected to 3 heat shock sessions during the 10-day feeding period. Left-hand panels demonstrate heat shock-induced expression of mRFP (red) in zebrafish. Right hand panels show vascular cholesterol deposits (green). White dashed lines trace the caudal vein in zebrafish. **d,** Quantification of vascular lipid deposits. Mean±SEM; n=4-11; *, $p<0.05$ (one-way ANOVA with Tukey's multiple comparison test).

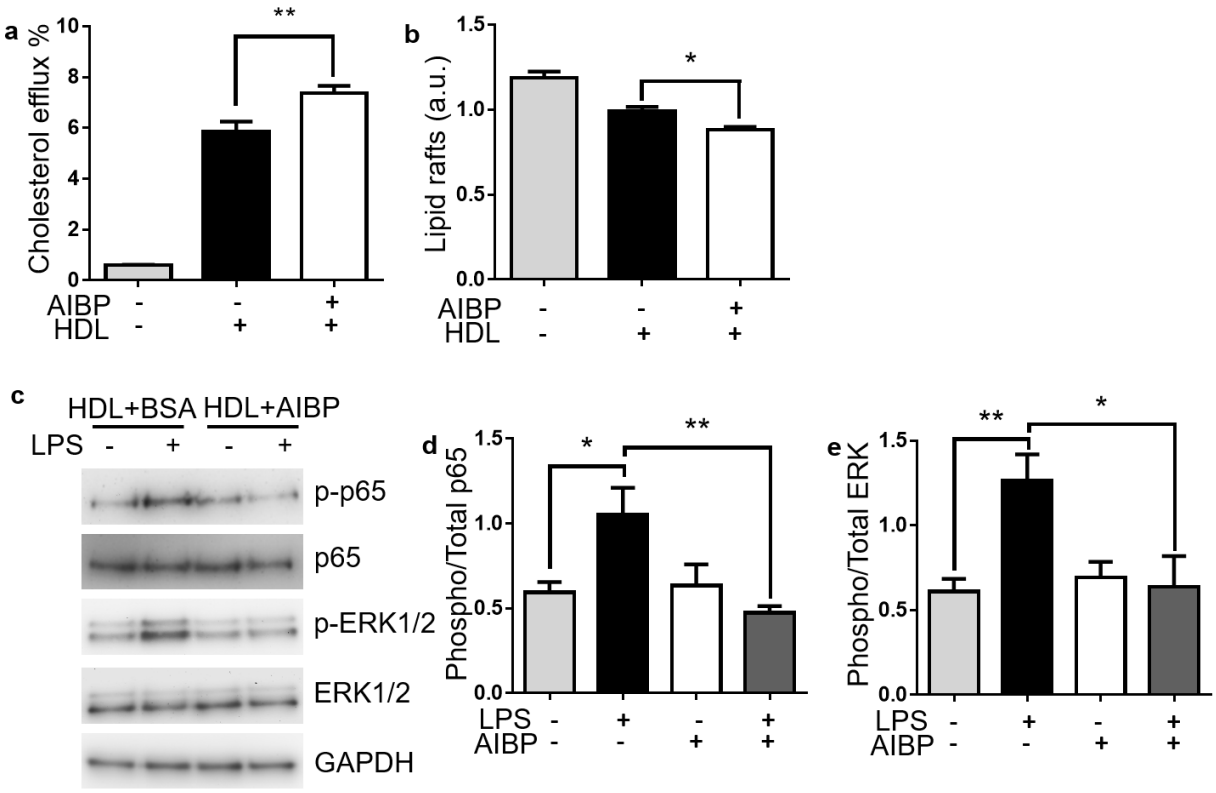


**Figure 1.7. AIBP facilitates cholesterol efflux and reduction in lipid rafts and inhibits macrophage inflammatory signaling. a,** Cholesterol efflux from macrophages. RAW264.7 macrophages were loaded for 24 hours with 2 µCi/mL [$^3$H]-cholesterol and then efflux was stimulated by 25 µg/mL HDL treatment in the presence or absence of 0.2 µg/mL AIBP for 4 hours (n=14 for HDL-containing samples; n=2 for media only). **b,** Cholera Toxin B binding was quantified via FACS to determine lipid raft content. RAW264.7 macrophages were loaded with acetylated LDL and treated for 4 hours with media only or 25 µg/mL HDL in the presence or absence of 0.2 µg/mL AIBP or BSA (n=3). **c,** RAW264.7 macrophages were stimulated with 10 ng/ml LPS for 30 min, in the presence of BSA or AIBP. Phosphorylation of p65 and ERK1/2 were assessed via gel electrophoresis and western blotting of cell lysates. **d,** Quantification of p65 phosphorylation (n=5). **e,** Quantification of ERK phosphorylation (n=6). Mean±SEM; **, $p<0.01$ ; *,$p<0.05$ (one-way ANOVA).

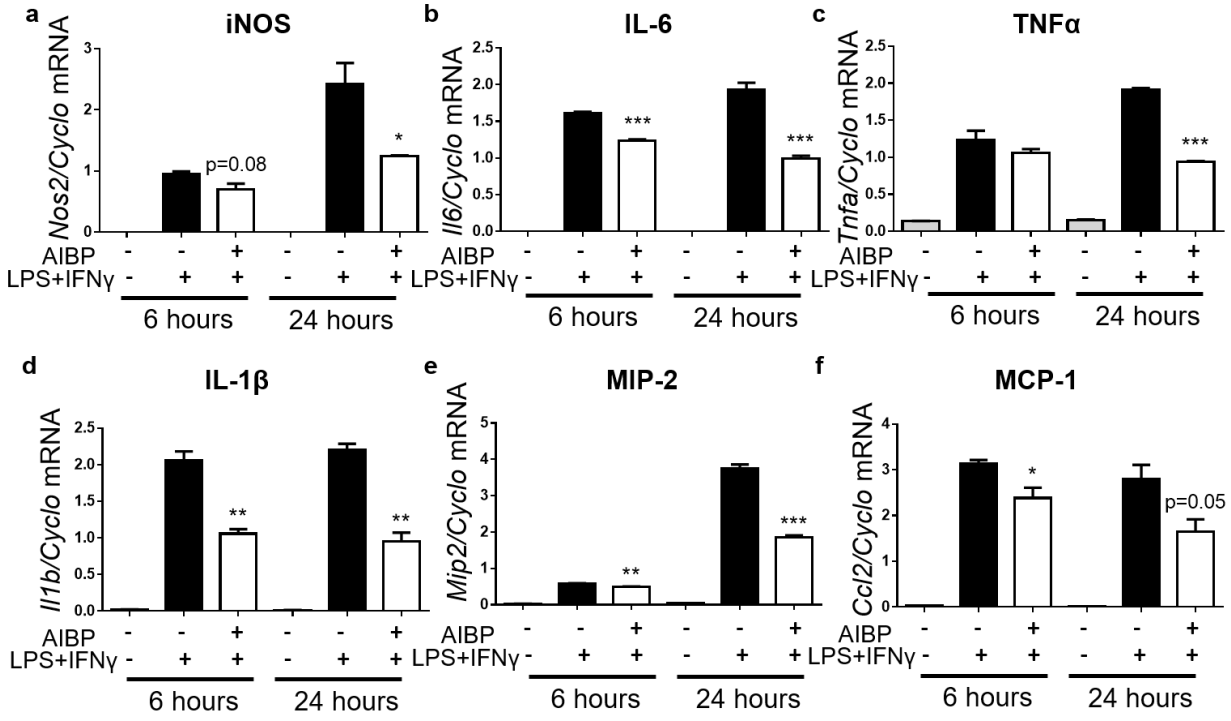


**Figure 1.8. AIBP suppresses macrophage inflammatory response. a-f,** RAW264.7 macrophages were stimulated with 10 ng/mL LPS and 50 ng/mL IFNγ in the presence of 0.2 μg/mL BSA or AIBP, for 6 or 24 hours. RNA was extracted from whole cell lysate. cDNA was synthesized from total RNA and used for quantitative PCR. Mean±SEM; n=3; ***, $p<0.001$; **, $p<0.01$; *, $p<0.05$ (Student's t-test).

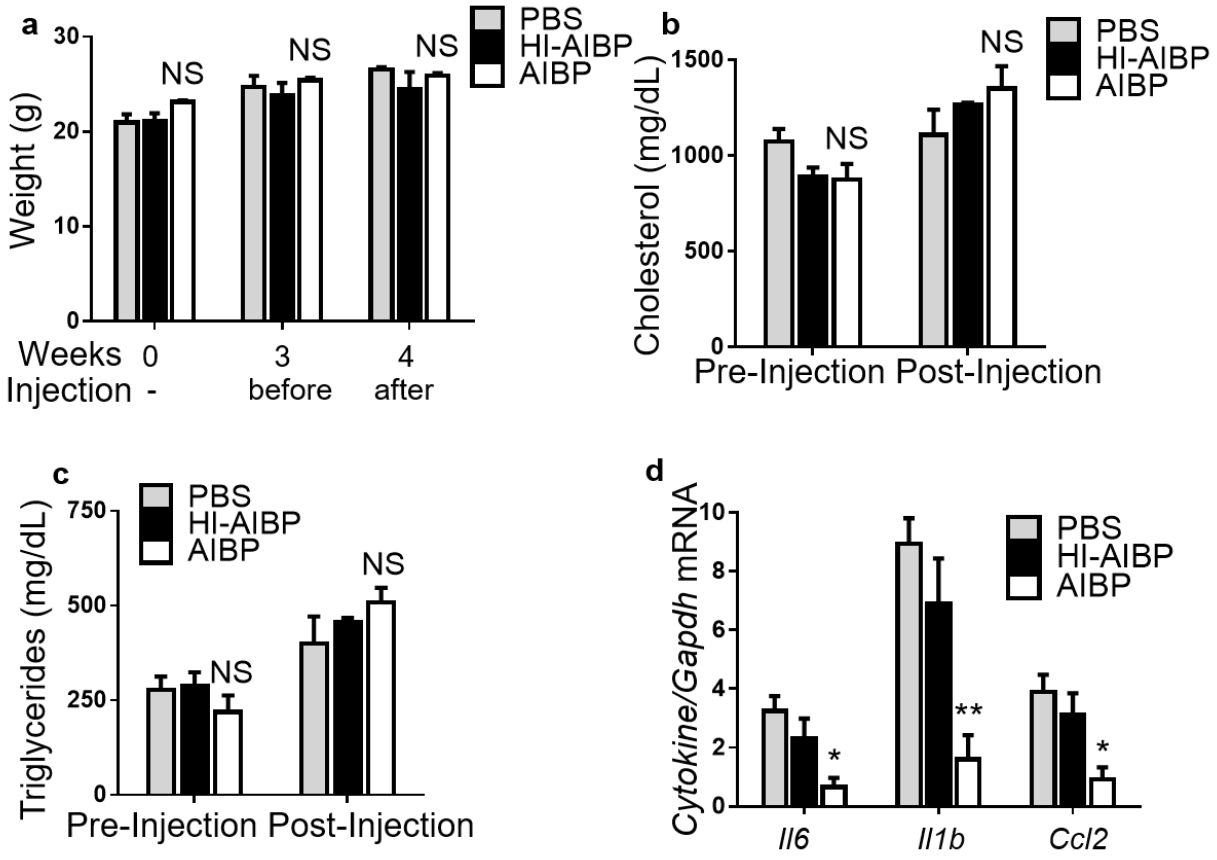


**Figure 1.9. Injections of recombinant AIBP suppress vascular inflammation *in vivo*.** *Ldlr*$^{-/-}$ mice were fed Western diet containing 1.25% cholesterol and 42% (kcal) fat for 4 weeks and i.v. injected with PBS, 0.5 µg AIBP or 0.5 µg heat inactivated (HI)-AIBP three times during last week of feeding. **a,** Body weight. **b,** Total plasma cholesterol before the start of injections (week 3) and in terminal blood (week 4). **c,** Plasma triglycerides. **d,** mRNA expression of inflammatory cytokines in whole aorta. Mean±SEM; n=3-4; **, $p<0.01$; *, $p<0.05$ (one-way ANOVA).

## Chapter References


Baigent, C., A. Keech, P. M. Kearney, L. Blackwell, G. Buck, C. Pollicino, A. Kirby, T. Sourjina, R. Peto, R. Collins and R. Simes (2005). "Efficacy and safety of cholesterol-lowering treatment: prospective meta-analysis of data from 90,056 participants in 14 randomised trials of statins." Lancet **366**(9493): 1267-1278.

Bodnar, J. S., A. Chatterjee, L. W. Castellani, D. A. Ross, J. Ohmen, J. Cavalcoli, C. Wu, K. M. Dains, J. Catanese, M. Chu, S. S. Sheth, K. Charugundla, P. Demant, D. B. West, P. de Jong and A. J. Lusis (2002). "Positional cloning of the combined hyperlipidemia gene Hyplip1." Nat Genet **30**(1): 110-116.

Choi, S. H. and H. N. Ginsberg (2011). "Increased very low density lipoprotein (VLDL) secretion, hepatic steatosis, and insulin resistance." Trends Endocrinol Metab **22**(9): 353-363.

Choi, S. H., P. Wiesner, F. Almazan, J. Kim and Y. I. Miller (2012). "Spleen tyrosine kinase regulates AP-1 dependent transcriptional response to minimally oxidized LDL." PLoS One **7**(2): e32378.

Chung, S., J. K. Sawyer, A. K. Gebre, N. Maeda and J. S. Parks (2011). "Adipose tissue ATP binding cassette transporter A1 contributes to high-density lipoprotein biogenesis in vivo." Circulation **124**(15): 1663-1672.

de Haan, W., A. Bhattacharjee, P. Ruddle, M. H. Kang and M. R. Hayden (2014). "ABCA1 in adipocytes regulates adipose tissue lipid content, glucose tolerance, and insulin sensitivity." J Lipid Res **55**(3): 516-523.

Fang, L., S. H. Choi, J. S. Baek, C. Liu, F. Almazan, F. Ulrich, P. Wiesner, A. Taleb, E. Deer, J. Pattison, J. Torres-Vazquez, A. C. Li and Y. I. Miller (2013). "Control of angiogenesis by AIBP-mediated cholesterol efflux." Nature **498**(7452): 118-122.

Fang, L., S. R. Green, J. S. Baek, S. H. Lee, F. Ellett, E. Deer, G. J. Lieschke, J. L. Witztum, S. Tsimikas and Y. I. Miller (2011). "In vivo visualization and attenuation of oxidized lipid accumulation in hypercholesterolemic zebrafish." J Clin Invest **121**(12): 4861-4869.

Fisher, E. A., J. E. Feig, B. Hewing, S. L. Hazen and J. D. Smith (2012). "High-density lipoprotein function, dysfunction, and reverse cholesterol transport." Arteriosclerosis, Thrombosis, and Vascular Biology **32**(12): 2813-2820.

Go, A. S., D. Mozaffarian, V. L. Roger, E. J. Benjamin, J. D. Berry, M. J. Blaha, S. Dai, E. S. Ford, C. S. Fox, S. Franco, H. J. Fullerton, C. Gillespie, S. M. Hailpern, J. A. Heit, V. J. Howard, M. D. Huffman, S. E. Judd, B. M. Kissela, S. J. Kittner, D. T. Lackland, J. H. Lichtman, L. D. Lisabeth, R. H. Mackey, D. J. Magid, G. M. Marcus, A. Marelli, D. B. Matchar, D. K. McGuire, E. R. Mohler, 3rd, C. S. Moy, M. E. Mussolino, R. W. Neumar, G. Nichol, D. K. Pandey, N. P. Paynter, M. J. Reeves, P. D. Sorlie, J. Stein, A. Towfighi, T. N. Turan, S. S. Virani, N. D. Wong, D. Woo, M. B. Turner, C. American Heart Association Statistics and S. Stroke Statistics (2014).

"Heart disease and stroke statistics--2014 update: a report from the American Heart Association." Circulation **129**(3): e28-e292.

Hartvigsen, K., C. J. Binder, L. F. Hansen, A. Rafia, J. Juliano, S. Horkko, D. Steinberg, W. Palinski, J. L. Witztum and A. C. Li (2007). "A diet-induced hypercholesterolemic murine model to study atherogenesis without obesity and metabolic syndrome." Arterioscler Thromb Vasc Biol **27**(4): 878-885.

Heinecke, J. W. (2012). "The not-so-simple HDL story: A new era for quantifying HDL and cardiovascular risk?" Nat Med **18**(9): 1346-1347.

Huang, X., A.-V. Hartley, Y. Yin, J. H. Herskowitz, J. J. Lah and K. J. Ressler (2013). "AAV2 production with optimized N/P ratio and PEI-mediated transfection results in low toxicity and high titer for in vitro and in vivo applications." Journal of Virological Methods **193**(2): 270-277.
Jha, K. N., I. A. Shumilin, L. C. Digilio, O. Chertihin, H. Zheng, G. Schmitz, P. E. Visconti, C. J. Flickinger, W. Minor and J. C. Herr (2008). "Biochemical and structural characterization of apolipoprotein A-I binding protein, a novel phosphoprotein with a potential role in sperm capacitation." Endocrinology **149**(5): 2108-2120.

Kim, F., M. Pham, E. Maloney, N. O. Rizzo, G. J. Morton, B. E. Wisse, E. A. Kirk, A. Chait and M. W. Schwartz (2008). "Vascular inflammation, insulin resistance, and reduced nitric oxide production precede the onset of peripheral insulin resistance." Arterioscler Thromb Vasc Biol **28**(11): 1982-1988.

Kim, J. H., S. R. Lee, L. H. Li, H. J. Park, J. H. Park, K. Y. Lee, M. K. Kim, B. A. Shin and S. Y. Choi (2011). "High cleavage efficiency of a 2A peptide derived from porcine teschovirus-1 in human cell lines, zebrafish and mice." PLoS One **6**(4): e18556.

Laatsch, A., M. Merkel, P. J. Talmud, T. Grewal, U. Beisiegel and J. Heeren (2009). "Insulin stimulates hepatic low density lipoprotein receptor-related protein 1 (LRP1) to increase postprandial lipoprotein clearance." Atherosclerosis **204**(1): 105-111.

Larach, D., E. deGoma and D. Rader (2012). "Targeting High Density Lipoproteins in the Prevention of Cardiovascular Disease?" Current Cardiology Reports **14**(6): 684-691.

Lawrence, T. and G. Natoli (2011). "Transcriptional regulation of macrophage polarization: enabling diversity with identity." Nat Rev Immunol **11**(11): 750-761.

Mao, R., S. Meng, Q. Gu, R. Araujo-Gutierrez, S. Kumar, Q. Yan, F. Almazan, K. A. Youker, Y. Fu, H. J. Pownall, J. P. Cooke, Y. I. Miller and L. Fang (2017). "AIBP Limits Angiogenesis Through gamma-Secretase-Mediated Upregulation of Notch Signaling." Circ Res **120**(11): 1727-1739.

Marbaix, A. Y., G. Noël, A. M. Detroux, D. Vertommen, E. Van Schaftingen and C. L. Linster (2011). "Extremely Conserved ATP- or ADP-dependent Enzymatic System for Nicotinamide Nucleotide Repair." Journal of Biological Chemistry **286**(48): 41246-41252.

O'Connell, B. J., M. Denis and J. Genest (2004). "Cellular physiology of cholesterol efflux in vascular endothelial cells." Circulation **110**(18): 2881-2888.

Plociennikowska, A., A. Hromada-Judycka, K. Borzecka and K. Kwiatkowska (2015). "Co-operation of TLR4 and raft proteins in LPS-induced pro-inflammatory signaling." Cell Mol Life Sci **72**(3): 557-581.

Raetz, C. R., T. A. Garrett, C. M. Reynolds, W. A. Shaw, J. D. Moore, D. C. Smith, Jr., A. A. Ribeiro, R. C. Murphy, R. J. Ulevitch, C. Fearns, D. Reichart, C. K. Glass, C. Benner, S. Subramaniam, R. Harkewicz, R. C. Bowers-Gentry, M. W. Buczynski, J. A. Cooper, R. A. Deems and E. A. Dennis (2006). "Kdo2-Lipid A of Escherichia coli, a defined endotoxin that activates macrophages via TLR-4." J Lipid Res **47**(5): 1097-1111.

Ritter, M., C. Buechler, A. Boettcher, S. Barlage, A. Schmitz-Madry, E. Orso, S. M. Bared, G. Schmiedeknecht, C. H. Baehr, G. Fricker and G. Schmitz (2002). "Cloning and characterization of a novel apolipoprotein A-I binding protein, AI-BP, secreted by cells of the kidney proximal tubules in response to HDL or ApoA-I." Genomics **79**(5): 693-702.

Rosenson, R. S., H. B. Brewer, W. S. Davidson, Z. A. Fayad, V. Fuster, J. Goldstein, M. Hellerstein, X. c. Jiang, M. C. Phillips, D. J. Rader, A. T. Remaley, G. H. Rothblat, A. R. Tall and L. Yvan-Charvet (2012). "Cholesterol Efflux and Atheroprotection: Advancing the Concept of Reverse Cholesterol Transport." Circulation **125**(15): 1905-1919.

Sears, D. D., P. D. Miles, J. Chapman, J. M. Ofrecio, F. Almazan, D. Thapar and Y. I. Miller (2009). "12/15-Lipoxygenase Is Required for the Early Onset of High Fat Diet-Induced Adipose Tissue Inflammation and Insulin Resistance in Mice." PLoS ONE **4**(9): e7250.

Shumilin, I. A., M. Cymborowski, O. Chertihin, K. N. Jha, J. C. Herr, S. A. Lesley, A. Joachimiak and W. Minor (2012). "Identification of unknown protein function using metabolite cocktail screening." Structure **20**(10): 1715-1725.

Steinberg, D., C. K. Glass and J. L. Witztum (2008). "Evidence Mandating Earlier and More Aggressive Treatment of Hypercholesterolemia." Circulation **118**(6): 672-677.

Stoletov, K., L. Fang, S. H. Choi, K. Hartvigsen, L. F. Hansen, C. Hall, J. Pattison, J. Juliano, E. R. Miller, F. Almazan, P. Crosier, J. L. Witztum, R. L. Klemke and Y. I. Miller (2009). "Vascular lipid accumulation, lipoprotein oxidation, and macrophage lipid uptake in hypercholesterolemic zebrafish." Circ Res **104**(8): 952-960.

Tall, A. R. and D. J. Rader (2018). "Trials and Tribulations of CETP Inhibitors." Circulation Research **122**(1): 106-112.

Tsimikas, S., A. Miyanohara, K. Hartvigsen, E. Merki, P. X. Shaw, M. Y. Chou, J. Pattison, M. Torzewski, J. Sollors, T. Friedmann, N. C. Lai, H. K. Hammond, G. S. Getz, C. A. Reardon, A.

C. Li, C. L. Banka and J. L. Witztum (2011). "Human oxidation-specific antibodies reduce foam cell formation and atherosclerosis progression." J Am Coll Cardiol **58**(16): 1715-1727.

Wada, J. and H. Makino (2016). "Innate immunity in diabetes and diabetic nephropathy." Nat Rev Nephrol **12**(1): 13-26.

Westerfield, M. (2007). The Zebrafish Book. A Guide for the Laboratory Use of Zebrafish (Danio rerio). Eugene, OR, University of Oregon Press.

Whetzel, A. M., J. M. Sturek, M. H. Nagelin, D. T. Bolick, A. K. Gebre, J. S. Parks, A. C. Bruce, M. D. Skaflen and C. C. Hedrick (2010). "ABCG1 deficiency in mice promotes endothelial activation and monocyte-endothelial interactions." Arterioscler Thromb Vasc Biol **30**(4): 809-817.

Zhang, M., L. Li, W. Xie, J. F. Wu, F. Yao, Y. L. Tan, X. D. Xia, X. Y. Liu, D. Liu, G. Lan, M. Y. Zeng, D. Gong, H. P. Cheng, C. Huang, Z. W. Zhao, X. L. Zheng and C. K. Tang (2016). "Apolipoprotein A-1 binding protein promotes macrophage cholesterol efflux by facilitating apolipoprotein A-1 binding to ABCA1 and preventing ABCA1 degradation." Atherosclerosis **248**: 149-159.

SUPPLEMENTAL DATA TO CHAPTER 1

**Supplemental Table 1.S1. High-fat, normal-cholesterol diet: Research Diets D12451**

| | % by weight | % kcal from | |
|---|---|---|---|
| Protein | 24 | 20 | |
| Carbohydrate | 41 | 35 | |
| Fat | 24 | 45 | |
| Kcal/g | | | 4.73 |

| Ingredient | Grams |
|---|---|
| Casein 30 mesh | 200 |
| L-Cystine | 3 |
| Corn Starch | 72.8 |
| Maltodextrin 10 | 100 |
| Sucrose | 172.8 |
| Cellulose BW200 | 50 |
| Soybean Oil | 25 |
| Lard | 177.5 |
| Mineral Mix S10026 | 10 |
| DiCalcium Phosphate | 13 |
| Calcium Carbonate | 5.5 |
| Potassium Citrate, 1 H2O | 16.5 |
| Vitamin Mix V10001 | 10 |
| Choline Bitartrate | 2 |
| FD&C Red Dye #40 | 0.05 |

**Supplemental Table 1.S2. High-fat, high-cholesterol (Western) diet: Teklad/Envigo TD.96121**

| | % by weight | % kcal from | |
|---|---|---|---|
| Protein | 17.3 | 15.2 | |
| Carbohydrate | 48.5 | 42.7 | |
| Fat | 21.2 | 42.0 | |
| Kcal/g | | | 4.5 |

| Ingredient | Grams |
|---|---|
| Casein | 195 |
| DL-Methionine | 3 |
| Sucrose | 341.46 |
| Corn Starch | 150 |
| Anhydrous Milkfat | 210 |
| Cholesterol | 12.5 |
| Cellulose | 39 |
| Mineral Mix AIN-76 (170915) | 35 |
| Calcium Carbonate | 4 |
| Vitamin Mix Teklad (40060) | 10 |
| Ethoxyquin (antioxidant) | 0.04 |

**Supplemental Table 1.S3. Normal-fat, high-cholesterol diet: Teklad/Envigo TD.97131**

| | % by weight | % kcal from | |
|---|---|---|---|
| Protein | 24.2 | 32.4 | |
| Carbohydrate | 40.5 | 54.2 | |
| Fat | 4.5 | 13.4 | |
| Kcal/g | | | 3.0 |

| Ingredient | Grams |
|---|---|
| Teklad Rodent Diet 8604 | 990 |
| Cholesterol | 10 |

**Supplemental Table 1.S4. qPCR primer sequences.**

| Gene | Forward Primer | Reverse Primer |
|---|---|---|
| Abca1 | GCC TTG GCA GTG TCC AAC ATC | TGT CTG AGA GAC AGA GTA GTC TTC |
| Abcg1 | AGG TCT CAG CCT TCT AAA GTT CCT C | TCT CTC GAA GTG AAT GAA ATT TAT CG |
| Abcg5 | TGG ATC CAA CAC CTC TAT GCT AAA | GGC AGG TTT TCT CGA TGA ACT G |
| Abcg8 | AGA GTT GCA TCC CCC TAG CC | TCC TTG ACA CAG GCA TGA AGC |
| ApoA-I | GGC ACG TAT GGC AGC AAG AT | CCA AGG AGG AGG ATT CAA ACT G |
| ApoB | TTC CAG CCA TGG GCA ACT TTA CCT | TAC TGC AGG GCG TCA GTG ACA AAT |
| Lrp1 | TGG TCT GAT GTG CGG ACT CA | AAC AGA TTT CGG GAG ACC CA |
| Hes1 | CTA CCC CAG CCA GTG TCA AC | AAG CGG GTC ACC TCG TTC AT |
| Pparg | ACG TGC AGC TAC TGC ATG TGA | AGA AGG AAC ACG TTG TCA GCG |
| Srebp2 | GTG CGC TCT CGT TTT ACT GAA GT | GTA TAG AAG ACG GCC TTC ACC AA |
| Srebp1c | GCA GCC ACC ATC TAG CCT G | CAG CAG TGA GTC TGC CTT GAT |
| Insig2a | CCC TCA ATG AAT GTA CTG AAG GAT T | TGT GAA GTG AAG CAG ACC AAT GT |
| Fasn | GGA GGT GGT GAT AGC CGG TAT | TGG GTA ATC CAT AGA GCC CAG |
| Acc | GCC TCC GTC AGC TCA GAT AC | ATG TGA AAG GCC AAA CCA TC |
| Elovl5 | ACA GGT GTG TGG GAA GGC AAA TA | GAG AAG TAG TAC CAC CAG AGG ACG |
| Gpat | GGC ATC TCG TAT GAT CGC AT | GCA AAA TCC ACT CGG ACG TA |
| Scd1 | CCG GAG ACC CTT AGA TCG A | TAG CCT GTA AAA GAT TTC TGC AAA CC |
| Pepck | GTG CTG GAG TGG ATG TTC GG | CTG GCT GAT TCT CTG TTT CAG G |
| Tnfa | CGA GTG ACA AGC CTG TAG CCC | GCA AAT CGG CTG ACG GTG TGG |
| Lpcat3 | GGG ACA AAT GGC TTA AGG TG | CTT TTC TTG GCA CCA TTG CT |
| Nos2 | GTT CTC AGC CCA ACA ATA CAA GA | GTG GAC GGG TCG ATG TCA C |
| Il6 | ACA ACC ACG GCC TCC CCT ACT T | ATC CAG TTT GGT AGC ATC CAT CAT |
| Il1b | GAC CTG GGC TGT CCT GAT GAG | GAA CGT CAC ACA CCA GCA GGT T |
| Mip2 | GCT CCT CAG TGC TGC ACT GGT | GGC TTC AGG GTC AAG GCA AAC T |
| Ccl2 | CCA CTC ACC TGC TGC TAC TCA T | GAA GAC CTT AGG GCA GAT GCA G |
| Cyclo | TGG AGA GCA CCA AGA CAG ACA | TGC CGG AGT CGA CAA TGA T |
| Gapdh | TCA CCA CCA TGG AGA AGG C | GCT AAG CAG TTG GTG GTG CA |

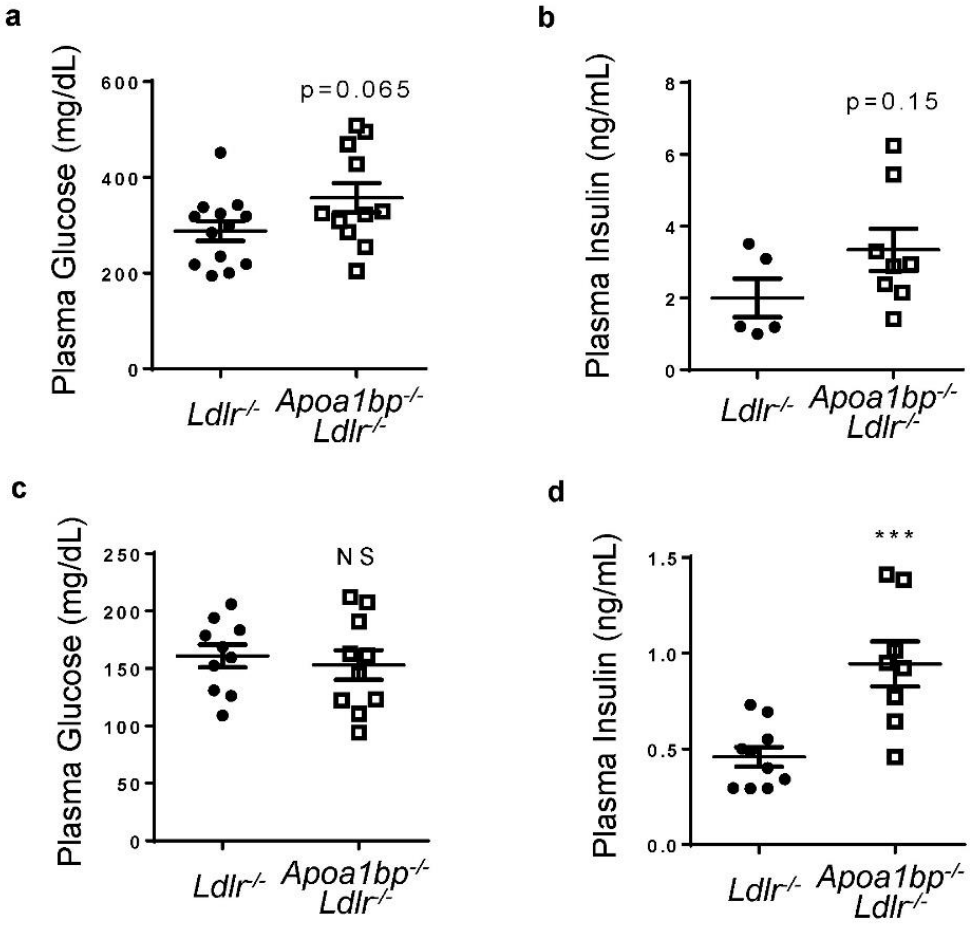


**Supplemental Figure 1.S1. Plasma glucose and insulin levels in AIBP-deficient mice fed a high-cholesterol or Western diet. a** and **b,** *Ldlr*$^{-/-}$ and *Apoa1bp*$^{-/-}$*Ldlr*$^{-/-}$ mice were fed Western diet for 12 weeks starting from age 8 weeks. Blood was collected at sacrifice, and plasma glucose (**a;** n=12-13) and insulin (**b;** n=5-8) levels were measured. **c** and **d,** *Ldlr*$^{-/-}$ and *Apoa1bp*$^{-/-}$ *Ldlr*$^{-/-}$ mice were fed a 1% cholesterol, normal fat diet for 16 weeks starting from age 8 weeks. Blood was collected at sacrifice, and plasma glucose (**c**) and insulin (**d**) levels were measured (n=10;). Mice were not fasted prior to sacrifice. Mean±SEM; ***, $p<0.001$ (Student's t-test).

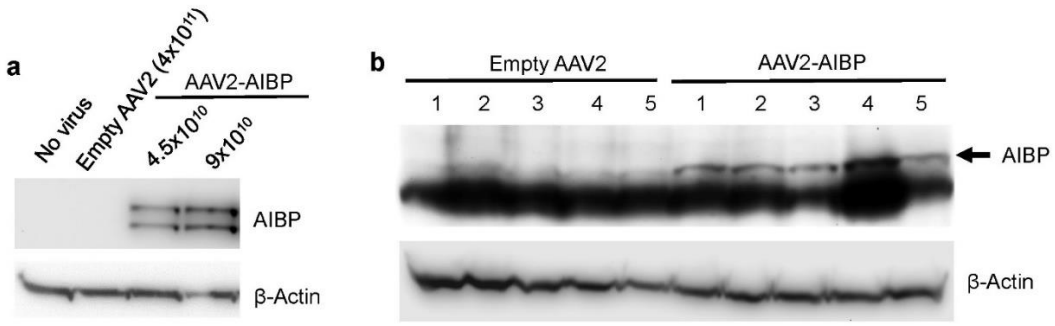


**Supplemental Figure 1.S2. AIBP expression in 293 cells and in liver of animals infected with AAV2-AIBP. a,** HEK293 cells were infected with empty AAV2 or AAV2-AIBP at indicated titers (gc/mL). At day 5 post-infection, cells were harvested, and cell lysates subjected to SDS-PAGE and immunoblot with an anti-His antibody. The lower band corresponds to AIBP from which FIB has been cleaved off. **b,** At the time of sacrifice, livers of mice infected with empty AAV2 or AAV2-AIBP were homogenized in RIPA buffer and subjected to SDS-PAGE and immunoblot with an anti-His antibody.

CHAPTER 2

# Role of AIBP in Metabolism


## Abstract

Little is known regarding the effects of AIBP on metabolism. AIBP-mediated cholesterol efflux depletes lipid rafts, an important signaling platform for numerous pathways, including inflammation, insulin signaling, and more. Additionally, an intracellular function for AIBP as an NAD(P)H-hydrate-epimerase has been proposed, which would give it a putative role in cellular metabolic regulation. Here we show that *in vivo*, mice lacking AIBP have altered whole-body metabolic function, including weight gain and elevated plasma lipids under high-fat dietary conditions. Additionally, mitochondrial function is impaired, as shown by decreased oxygen consumption and oxidative phosphorylation complex expression. Supporting the intracellular epimerase function proposal, we found that livers from AIBP-deficient mice exhibited increased buildup of NAD(P)H-hydrate. We conclude that AIBP plays an important role in metabolism *in vivo*.


## Introduction

Inflammation shares a close connection with metabolic disorders. Unlike a typical inflammatory response which has a danger-associated trigger followed by resolution, obesity-related inflammation is an ongoing process at a subacute level (McNelis and Olefsky 2014). Obesity-related inflammation has been linked to defects in insulin signaling and insulin resistance, and it can be present in multiple organ systems (Brestoff and Artis 2015, Saltiel and Olefsky 2017). During obesity, macrophage polarization shifts from homeostasis-oriented M2

macrophages to inflammatory M1 macrophages, ultimately becoming part of a chronic inflammatory circuit (Saltiel and Olefsky 2017). Inflammation is a critical mediator of metabolic defects; disruption of NF-κB or JNK signaling can rescue the insulin resistance phenotype normally associated with obesity (Saltiel and Olefsky 2017). TNFα is one key factor; it is a negative regulator of insulin signaling that has increased secretion from obese WAT, and genetic knockout of *Tnfa* protected mice against diet-induced insulin resistance (McNelis and Olefsky 2014, Brestoff and Artis 2015). Interestingly the TNF receptor requires recruitment to lipid rafts in order to signal, therefore efflux-mediated disruption of lipid rafts may alter signaling levels (Legler, Micheau et al. 2003).

In addition to the inflammatory feedback circuits already present in the body, diet-induced inflammation is an important consideration as well. Dietary lipid species and free fatty acids can activate pro-inflammatory and macrophage-recruiting signaling pathways, further contributing to the chronic inflammatory state in obesity (Saltiel and Olefsky 2017). Toll-Like Receptor 4 (TLR4) has been found to produce inflammatory signaling when activated by dietary saturated fatty acids, its specific deletion in hematopoietic cells alone is sufficient to protect against diet-induced insulin resistance (Huang, Rutkowsky et al. 2012, McNelis and Olefsky 2014). Dietary lipids can cause inflammation via other mechanisms than directly signaling; one example is when elevated dietary triglycerides accumulate in the white adipose tissue (WAT), causing it to expand and produce leptin which further stimulates inflammation (Brestoff and Artis 2015). This hypertrophy also leads to hypoxia and its related downstream inflammatory mediators (Brestoff and Artis 2015).

Intriguingly, depletion of liver-resident macrophages (Kupffer cells) protects against HFD-induced hepatic TG accumulation without affecting plasma TGs (Huang, Metlakunta et al.

2010). Mice injected with LPS develop rapid elevation in hepatic lipid levels and suppressed expression of fatty acid metabolism genes (Ohhira, Motomura et al. 2007). Co-culture experiments of hepatocytes in the presence or absence of Kupffer cells reveal that while LPS does not directly stimulate hepatocyte damage, Kupffer cells polarized towards M1 status by LPS induce hepatocyte TG accumulation and a reduction in insulin signaling pathway sensitivity (Huang, Metlakunta et al. 2010). This effect appears to be TNFα-mediated; neutralizing antibodies against the cytokine improved the adverse effects observed previously, but antibodies against other M1 cytokines such as IL-1β, IL-6, and IFNγ did not (Huang, Metlakunta et al. 2010). Mice reconstituted with hematopoietic cells that cannot polarize into M2 macrophages, and are thus more inflammatory, develop greater glucose intolerance than those receiving wildtype cells (Odegaard, Ricardo-Gonzalez et al. 2008).

In addition to the role of extracellular AIBP in inflammation-related metabolism, intracellular AIBP has been postulated to have implications as well. AIBP is proposed to be a NAD(P)H-hydrate (NAD(P)HX) epimerase, meaning that it can convert NADH(P)X between its (R) and (S)-epimers (Marbaix, Noel et al. 2011). NAD(P)HX is formed spontaneously and by a side reaction of GAPDH, and it inhibits several key dehydrogenases (Van Schaftingen, Rzem et al. 2013). The enzyme Carkd is able to repair NAD(P)HX back to its standard dehydrated form, but only acts on the (S)-epimer (Marbaix, Noel et al. 2011). AIBP is therefore required for rescue of the (R)-epimer, by converting it to (S) and allowing its dehydration by Carkd.

The NAD cycle is tightly regulated. As an example, when DNA damage induces PARP-1 activity, a major NAD+ consumer, this decrease in NAD+ availability is sufficient to impair glycolysis and mitochondrial function (Bai and Canto 2012). Pathways dependent on NAD+, such as mitochondrial function and lipid oxidation, are sensitive enough to its availability that

they follow the same circadian pattern as NAD+ levels (Peek, Affinati et al. 2013). Thus the proposed importance of intracellular AIBP is twofold; by enabling NAD(P)HX repair it rescues NAD+ from becoming trapped as hydrate and protects NAD balance, while preventing dehydrogenase inhibition by NAD(P)HX. Indeed, in fibroblasts from human subjects with mutations in *APOA1BP* (also referred to as *NAXE*), NAD(P)HX levels were significantly increased (Kremer, Danhauser et al. 2016). These patients were also found to have decreased OXPHOS activity, elevated lactate levels, and reduced mitochondrial activity (Kremer, Danhauser et al. 2016). The aim of our studies was to investigate the potential roles of AIBP on metabolism *in vivo*, in tandem with the experiments described in Chapter 1.

## Methods

### *Animals and diets*

All animal experiments were conducted according to protocols approved by the Institutional Animal Care and Use Committee of the University of California, San Diego. Mice were housed up to 5 per standard cage at room temperature and maintained on a 12:12 hour light:dark cycle, with lights on at 07:00. Both food and water were available ad libitum. Wild type C57BL/6 and *Ldlr*$^{-/-}$ mice were initially purchased from Jackson Lab (Bar Harbor, ME) and bred in-house for experiments. *Apoa1bp*$^{-/-}$ mice were generated in our group as previously described (Mao, Meng et al. 2017) and cross-bred with *Ldlr*$^{-/-}$ mice. *Apoa1bp*$^{-/-}$*Ldlr*$^{-/-}$ mice develop and breed normally. For metabolic studies, mice on a C57BL/6 background were fed a high-fat diet (Research Diets D12451) containing 45% kcal from fat, starting at age 10 weeks. For metabolic and atherosclerosis studies, mice on an *Ldlr*$^{-/-}$ background were fed either a Western Diet (Teklad TD.96121) containing 42% kcal from fat (21% milkfat) and 1.25% cholesterol or a high-

cholesterol, normal-fat diet (Teklad TD.97131) containing 1% cholesterol, starting at age 8 weeks.

*Metabolic cage testing*

Testing was performed after 6 weeks of high fat feeding, using an Oxymax CLAMS system.

*Lipids and lipoprotein profile*

Blood was collected from mice into EDTA tubes upon sacrifice and plasma was collected following centrifugation.

*Western blotting*

Cell and tissue lysates were subjected to gel electrophoresis and immunoblot as described (Choi, Wiesner et al. 2012). Antibody cocktail specific to OXPHOS complexes was obtained from Invitrogen (#45-7999).

*NAD(P)HX metabolite measurements*

Metabolite measurements were performed by the West Coast Metabolomics Center, University of California, Davis. 100mg samples were analyzed for each liver. Samples were extracted by adding 400 µL of 50 mm ammonium acetate, pH 7.0, and homogenizing with a SPEX SamplePrep Geno/Grinder 2010 for 2 min at 1,250 rpm with 1.6-mm steel balls. The homogenate was transferred to a fresh 1.5-mL tube; the steel balls were washed with 600 µL of 3:1 acetonitrile/50 mm ammonium acetate, pH 7.0, and the wash was combined with the homogenate. Samples were centrifuged to clear, and the supernatant was transferred to 2-mL

tubes containing 900 µL of chloroform. Samples were vortexed for 20 s and centrifuged to separate the phases. The aqueous phase (550 µL) was transferred to a fresh 1.5-mL tube, lyophilized overnight, redissolved in 50 µL of 50 mm ammonium acetate, pH 7.0, and analyzed by LC-MS. Chromatography was performed on an Agilent 1290 Infinity LC System (Agilent Technologies). Samples were maintained at 4°C in the autosampler and 5 µL of sample material was injected onto a Polaris 3 C18-A 150 × 2.0 mm HPLC column kept at ambient temperature. Mobile phase A consisted of 50 mm ammonium acetate in water, pH 7.0, and mobile phase B consisted of acetonitrile. Target metabolites were eluted from the column using the following gradient: 0 to 5 min, 0% B; 5 to 20 min, linear gradient to 5% B; 20 to 25 min, linear gradient to 100% B; and 25 to 26 min, linear gradient to 0% B. Re-equilibration time was 14 min, and flow rate was held at 0.25 mL/min throughout the method. Metabolites were detected with an Agilent 6530 accurate-mass quadrupole time-of-flight mass spectrometer equipped with an Agilent Jet Stream electrospray ionization source. Mass spectrometry data were acquired in negative ionization mode from 100 to 1100 mass-to-charge ratio with a 2 spectra/s scan rate. Mass calibration was maintained by constant infusion of reference ions at 119.036320 and 980.016375 mass-to-charge ratio. Target analytes were identified based on retention time and accurate mass matching to authentic standards.

## Results

*Weight and lipid phenotypes in AIBP-deficient mice are diet- and background strain-dependent*

Atherosclerosis studies in mice are most often performed on either *Ldlr*$^{-/-}$ or *Apoe*$^{-/-}$ mice in order to facilitate lesion development. While our atherosclerosis cohorts are on an *Ldlr*$^{-/-}$ background, our initial metabolic study uses the C57BL/6 strain. Mice on a C57BL/6

background responded differently than those on an *Ldlr*$^{-/-}$ background to a diet with increased fat content, either a high-fat diet (HFD) or high fat plus cholesterol (WD) respectively (Fig. 1). While both strains of AIBP knockout gained more weight than wildtype controls (Fig. 1A), only the *Ldlr*$^{-/-}$ background resulted in increased plasma triglycerides (Fig. 1C). Within the same genetic background diet content plays an important role as well; *Ldlr*$^{-/-}$ mice fed a high-cholesterol diet (HCD) were protected against the weight gain developed on a high-fat high-cholesterol WD (Fig. 1A).

*Altered metabolic parameters in AIBP-deficient mice fed a high-fat diet*

To investigate the diet-induced weight gain observed in our *Apoa1bp*$^{-/-}$ mice, we performed metabolic cage testing of mice on a C57BL/6 background fed a HFD. Food intake was comparable between the genotypes, as was water consumption (Fig. 2A, B). Increased movement was not accountable for the weight difference; *Apoa1bp*$^{-/-}$ mice had similar levels of motion and ambulatory activity (Fig. 2C-E). However, *Apoa1bp*$^{-/-}$ mice consumed less oxygen and produced less carbon dioxide, suggesting an overall reduction in metabolic activity (Fig. 3A, B). Respiratory Exchange Ratio was not significantly altered, while heat production showed a trend of reduction (Fig. 3C, D).

*Oxidative phosphorylation complex expression is reduced in AIBP-deficient mice*

Alterations in OXPHOS complex activity were previously described in muscle biopsy from a human patient with mutated *Apoa1bp* (Kremer, Danhauser et al. 2016). To determine if this mitochondrial phenotype replicated in our mouse model, we examined OXPHOS complex expression in the liver, another highly metabolic tissue. Indeed, complex V was reduced in

AIBP-deficient mice in both C57BL/6 background/HFD and *Ldlr*$^{-/-}$ background/WD cohorts (Fig. 4A, B). However, complex I was only reduced in the *Ldlr*$^{-/-}$ background/WD cohort, and complexes II-IV were unchanged.

*Hepatic accumulation of NAD(P)HX*

While AIBP has been described as an NAD(P)HX epimerase in several publications, none has conclusively shown its relevance using an *in vivo* model (Marbaix, Noel et al. 2011, Van Schaftingen, Rzem et al. 2013, Marbaix, Tyteca et al. 2014, Kremer, Danhauser et al. 2016). To investigate this, we analyzed the relative levels of NAD and NADP metabolites in the livers of mice on a *Ldlr*$^{-/-}$ background/WD. Interestingly, NADPHX did not have increased hepatic accumulation of (R) or (S) epimers, only its cyclic form was significantly elevated in AIBP-deficient mice (Fig. 5A). This contrasts with NADHX, in which all three forms were increased (Fig. 5B). For reasons that remain unclear, NADP and NADPH were both increased as well (Fig. 5C). NAD and NADH were reduced in the knockout mice (Fig. 5D), supporting the hypothesis that NAD had become "trapped" in its hydrated form.

**Discussion**

In this study we investigated the *in vivo* metabolic role of AIBP, a function that has been proposed in the literature but not characterized. We found numerous metabolic abnormalities in mice lacking AIBP expression. *Apoa1bp*$^{-/-}$ mice have increased propensity towards diet-induced weight gain, decreased metabolic activity, and altered mitochondrial properties. Additionally, they accumulate toxic NAD(P) metabolites in the liver. One interesting point is that both the diet

fed and the genetic background of the mice resulted in strikingly different outcomes across all of our studies.

The enhanced weight gain observed in *Apoa1bp*$^{-/-}$ mice appears to be caused by a metabolic shift. Knockout mice had similar food intake and activity levels as control mice, ruling out excess nutrient intake or active energy expenditure as a cause. Data on $VO_2$ consumption and $VCO_2$ production data from metabolic cage testing provide more insight; both are decreased without a significant change in fuel source as indicated by Respiratory Exchange Ratio (RER). This strongly suggests suppressed mitochondrial activity in AIBP-deficient mice, as mitochondrial metabolism accounts for ~90% of all oxygen consumption (Rolfe and Brown 1997). We also found these mice to have reduced expression of several mitochondrial complex proteins, further supporting this observation.

One possibility which we did not investigate in this study is that AIBP plays a role in nutrient absorption across the gut. While no link between AIBP and intestinal absorption has been published, ABCA1 has been found to influence gut cholesterol uptake (Temel, Lee et al. 2005). As AIBP has been shown to stabilize ABCA1 protein levels, it is possible that *Apoa1bp*$^{-/-}$ mice may have altered cholesterol absorption from their dietary intake, despite having equal food consumption to controls (Zhang, Li et al. 2016). This is an important area for further study.

We performed three separate diet studies on two different genetic backgrounds. Despite the background difference, fat feeding produced a similar phenotype. Both HFD and WD led to increased body weight in *Apoa1bp*$^{-/-}$ mice, while a diet high in cholesterol but containing normal fat levels did not. This weight gain may be due to several different mechanisms, but one of particular note is inflammatory signaling by dietary fats. Saturated fatty acids from the diet can signal directly via TLR4, and indirect mechanisms such as adipocyte stimulation are

inflammatory as well (Huang, Rutkowsky et al. 2012, McNelis and Olefsky 2014, Brestoff and Artis 2015, Saltiel and Olefsky 2017). As discussed in chapter 1, AIBP is a suppressor of inflammation, so knockout mice would likely be more susceptible to fat-induced inflammatory signaling and resulting downstream metabolic perturbations. Additionally, elevated delivery of fatty acids to the liver has been shown to induce mitochondrial oxidative metabolism, oxidative stress, and inflammation, linking our observations on diet effect to the inflammation and mitochondrial phenotypes also observed (Satapati, Kucejova et al. 2016).

While AIBP has been characterized *in vitro* as an NAD(P)H-hydrate epimerase, the only published data from live subjects was taken from fibroblasts in two human patients with differing *Apoa1bp* mutations (Marbaix, Noel et al. 2011, Marbaix, Tyteca et al. 2014, Kremer, Danhauser et al. 2016). Due to the nature of these samples, it is difficult to draw strong conclusions regarding AIBP's epimerase function. Our study is the first to investigate *in vivo* accumulation of NAD(P) metabolites with sufficient statistical power, using *Apoa1bp*$^{-/-}$*Ldlr*$^{-/-}$ mice. We found that both NADHX and NADPHX accumulated in the liver, although there was epimer variability between the two. Interestingly, while NADHX increases were coupled with NAD decreases, the opposite was observed for NADP. There are two caveats to our NAD(PH)X study; mouse-to-mouse variability was dramatic and all values are relative. More thorough characterization is necessary to confirm our findings.

Taken together, our data supports the hypothesis that AIBP is a metabolic regulator *in vivo*. We found broad effects of AIBP knockout on metabolic parameters including body weight, mitochondrial function, and metabolite levels. Further characterization of the mechanism underlying AIBP-mediated metabolic regulation is an important research area for the future.

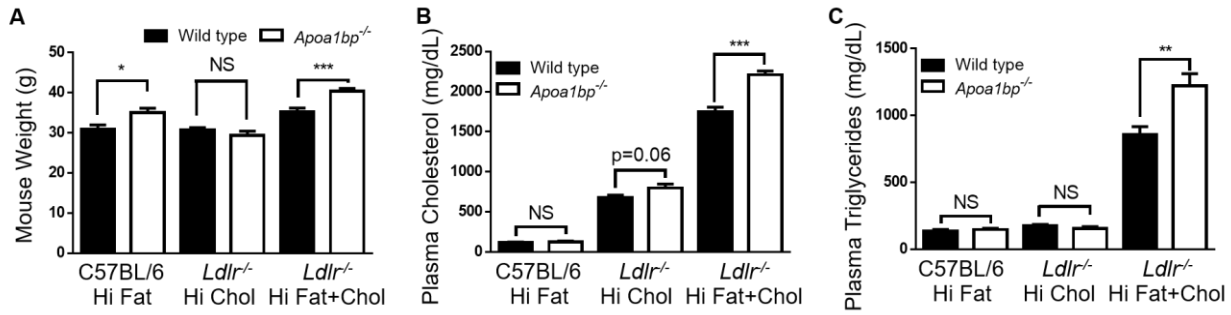


**Figure 2.1. Comparison of diet effects in *Apoa1bp*$^{-/-}$ mice.** C57BL/6 and *Apoa1bp*$^{-/-}$ mice or *Ldlr*$^{-/-}$ and *Apoa1bp*$^{-/-}$*Ldlr*$^{-/-}$ mice were fed the indicated diets. Hi fat diet is 10 weeks on 45% kcal from fat, 0.02% cholesterol. High chol diet is 16 weeks on 13.4% kcal from fat, 1% cholesterol. High fat+chol diet is 12 weeks on 42% kcal from fat, 1.25% cholesterol. A, Mouse weights. B, Plasma cholesterol and (C) triglycerides. N=10-13, Mean±SEM; ***,p<0.001 ; **,p<0.01 ; *,p<0.05 (t-test).

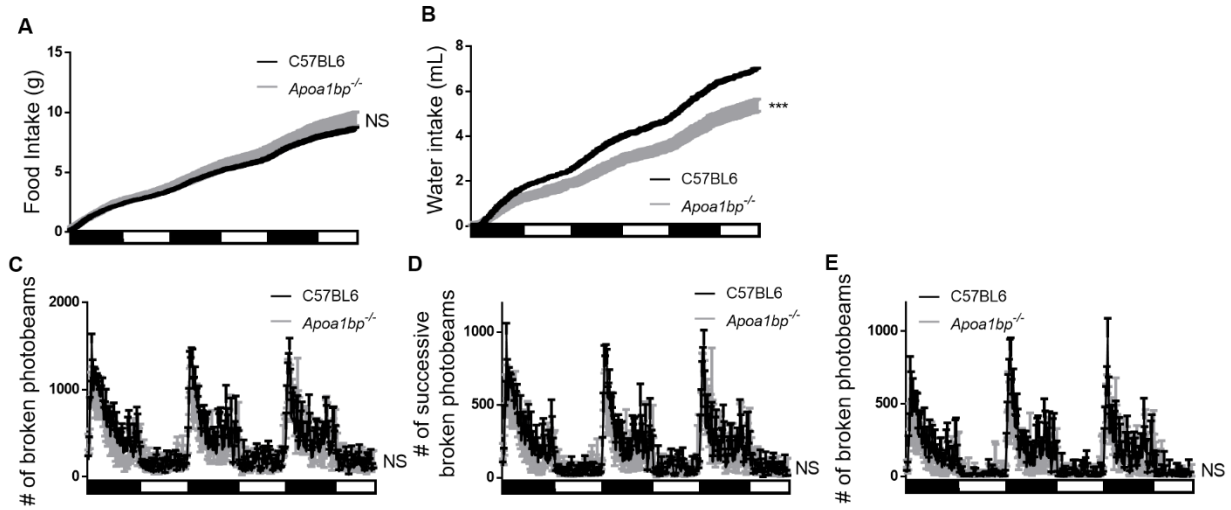


**Figure 2.2. Nutrient intake and activity of *Apoa1bp*$^{-/-}$ mice.** C57BL/6 and *Apoa1bp*$^{-/-}$ were fed a high fat diet for 6 weeks containing 45% kcal from fat, at which time metabolic cage testing was performed. A, Food intake. B, Water intake. C, Total horizontal activity. D, Ambulatory horizontal activity. E, Total vertical activity. N=10-12, Mean±SEM; ***,p<0.001 ; **,p<0.01 ; *,p<0.05 (2-way ANOVA).

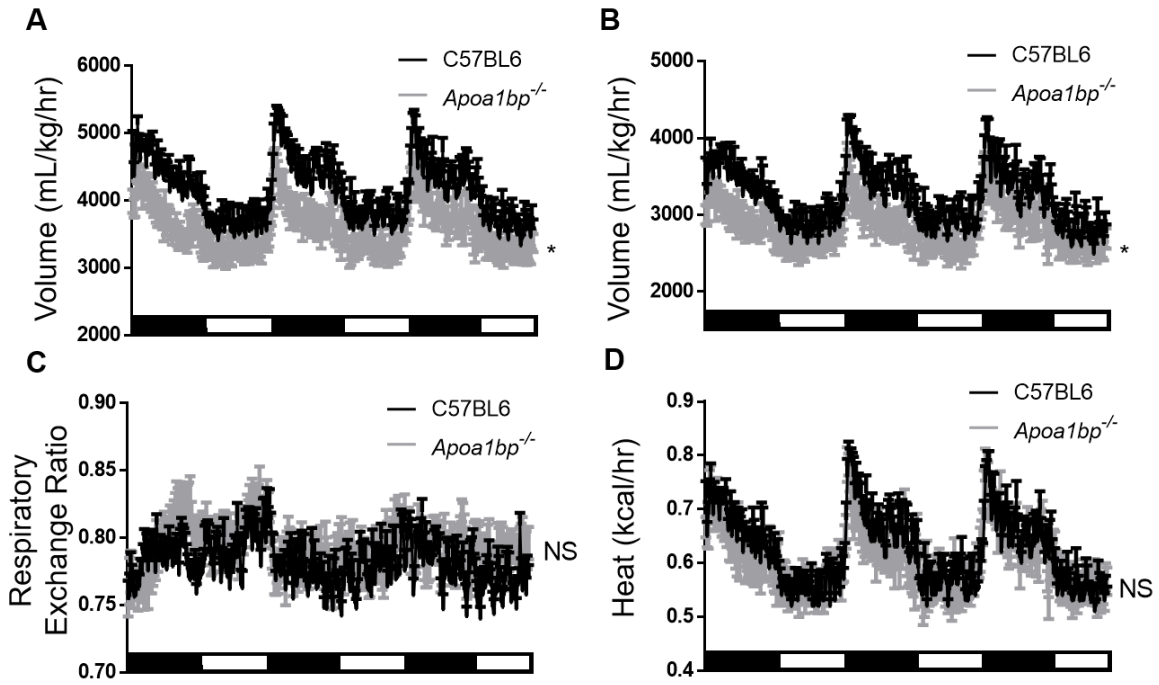


**Figure 2.3. Metabolic parameters of *Apoa1bp*$^{-/-}$ mice.** C57BL/6 and *Apoa1bp*$^{-/-}$ were fed a high fat diet for 6 weeks containing 45% kcal from fat, at which time metabolic cage testing was performed. A, VO2 consumption. B, VCO2 production. C, Respiratory exchange ratio. D, Heat production. N=10-12, Mean±SEM; *,p<0.05 (2-way ANOVA).

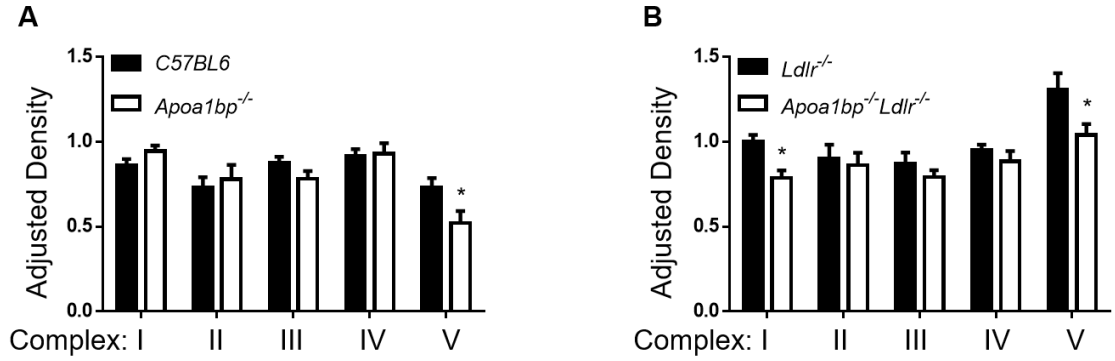


**Figure 2.4. Oxidative phosphorylation complex expression in *Apoa1bp*$^{-/-}$ mice.** Livers from mice fed the indicated diet were homogenized in RIPA buffer and analyzed for oxidative phosphorylation complex expression via Western blot densitometry. Densities were normalized to β-actin. A, C57BL/6 and *Apoa1bp*$^{-/-}$ mice were fed a high fat diet containing 45% kcal from fat for 10 weeks. B, *Ldlr*$^{-/-}$ and *Apoa1bp*$^{-/-}$*Ldlr*$^{-/-}$ mice were fed a Western diet containing 42% kcal from fat and 1.25% cholesterol for 12 weeks. N=6, Mean±SEM; *,p<0.05 (t-test).

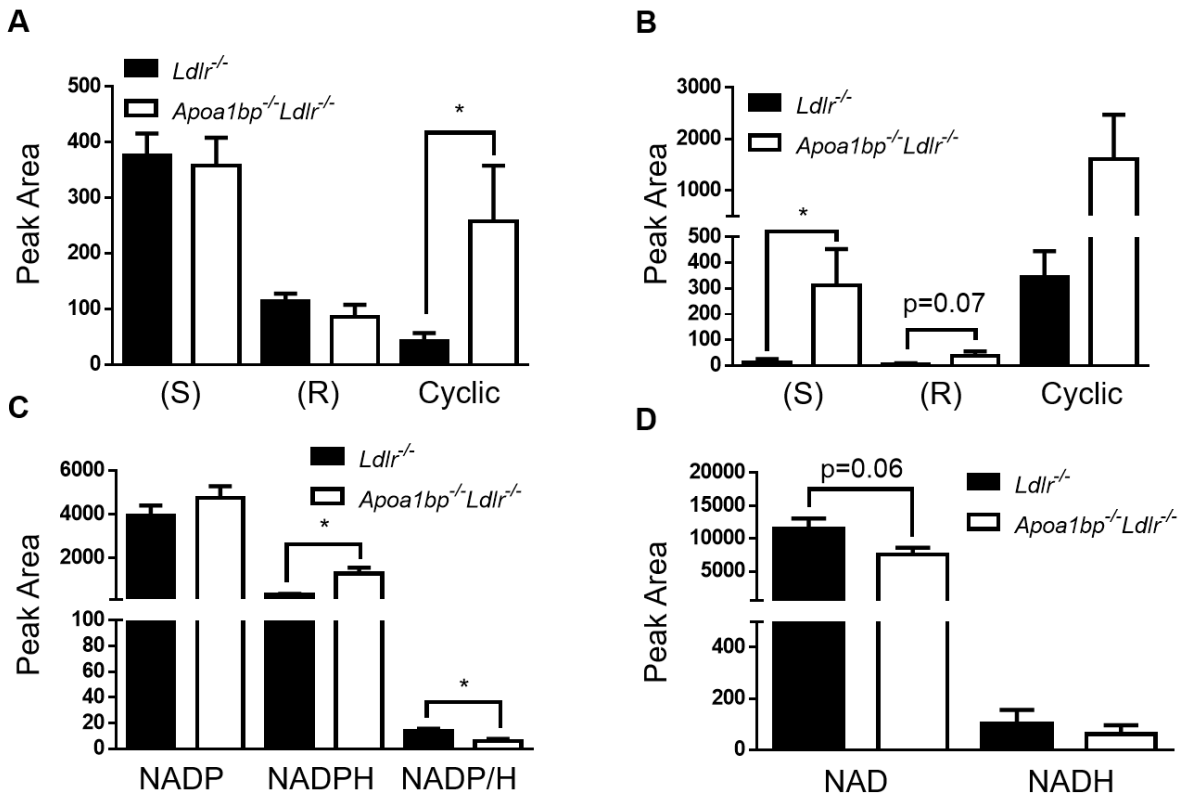


**Figure 2.5. NAD(P) metabolite differences in *Apoa1bp*$^{-/-}$ mice.** *Ldlr*$^{-/-}$ and *Apoa1bp*$^{-/-}$*Ldlr*$^{-/-}$ mice were fed a Western diet containing 1.25% cholesterol and 42% fat for 12 weeks starting from age 8 weeks. Livers were analyzed via LC-MS for the presence of various NAD(P) metabolites. A, NADPHX. B, NADHX. C, NADP and NADPH. NADP/H ratio is also shown. D, NAD and NADH. N=10-12, Mean±SEM; *,$p<0.05$ (t-test).

**Chapter References**

Bai, P. and C. Canto (2012). "The role of PARP-1 and PARP-2 enzymes in metabolic regulation and disease." Cell Metab **16**(3): 290-295.

Brestoff, J. R. and D. Artis (2015). "Immune regulation of metabolic homeostasis in health and disease." Cell **161**(1): 146-160.

Choi, S. H., P. Wiesner, F. Almazan, J. Kim and Y. I. Miller (2012). "Spleen tyrosine kinase regulates AP-1 dependent transcriptional response to minimally oxidized LDL." PLoS One **7**(2): e32378.

Huang, S., J. M. Rutkowsky, R. G. Snodgrass, K. D. Ono-Moore, D. A. Schneider, J. W. Newman, S. H. Adams and D. H. Hwang (2012). "Saturated fatty acids activate TLR-mediated proinflammatory signaling pathways." J Lipid Res **53**(9): 2002-2013.

Huang, W., A. Metlakunta, N. Dedousis, P. Zhang, I. Sipula, J. J. Dube, D. K. Scott and R. M. O'Doherty (2010). "Depletion of liver Kupffer cells prevents the development of diet-induced hepatic steatosis and insulin resistance." Diabetes **59**(2): 347-357.

Kremer, L. S., K. Danhauser, D. Herebian, D. Petkovic Ramadza, D. Piekutowska-Abramczuk, A. Seibt, W. Muller-Felber, T. B. Haack, R. Ploski, K. Lohmeier, D. Schneider, D. Klee, D. Rokicki, E. Mayatepek, T. M. Strom, T. Meitinger, T. Klopstock, E. Pronicka, J. A. Mayr, I. Baric, F. Distelmaier and H. Prokisch (2016). "NAXE Mutations Disrupt the Cellular NAD(P)HX Repair System and Cause a Lethal Neurometabolic Disorder of Early Childhood." Am J Hum Genet **99**(4): 894-902.

Legler, D. F., O. Micheau, M. A. Doucey, J. Tschopp and C. Bron (2003). "Recruitment of TNF receptor 1 to lipid rafts is essential for TNFalpha-mediated NF-kappaB activation." Immunity **18**(5): 655-664.

Mao, R., S. Meng, Q. Gu, R. Araujo-Gutierrez, S. Kumar, Q. Yan, F. Almazan, K. A. Youker, Y. Fu, H. J. Pownall, J. P. Cooke, Y. I. Miller and L. Fang (2017). "AIBP Limits Angiogenesis Through gamma-Secretase-Mediated Upregulation of Notch Signaling." Circ Res.

Marbaix, A. Y., G. Noel, A. M. Detroux, D. Vertommen, E. Van Schaftingen and C. L. Linster (2011). "Extremely conserved ATP- or ADP-dependent enzymatic system for nicotinamide nucleotide repair." J Biol Chem **286**(48): 41246-41252.

Marbaix, A. Y., D. Tyteca, T. D. Niehaus, A. D. Hanson, C. L. Linster and E. Van Schaftingen (2014). "Occurrence and subcellular distribution of the NADPHX repair system in mammals." Biochem J **460**(1): 49-58.

McNelis, J. C. and J. M. Olefsky (2014). "Macrophages, immunity, and metabolic disease." Immunity **41**(1): 36-48.

Odegaard, J. I., R. R. Ricardo-Gonzalez, A. Red Eagle, D. Vats, C. R. Morel, M. H. Goforth, V. Subramanian, L. Mukundan, A. W. Ferrante and A. Chawla (2008). "Alternative M2 activation of Kupffer cells by PPARdelta ameliorates obesity-induced insulin resistance." Cell Metab **7**(6): 496-507.

Ohhira, M., W. Motomura, M. Fukuda, T. Yoshizaki, N. Takahashi, S. Tanno, N. Wakamiya, Y. Kohgo, S. Kumei and T. Okumura (2007). "Lipopolysaccharide induces adipose differentiation-related protein expression and lipid accumulation in the liver through inhibition of fatty acid oxidation in mice." J Gastroenterol **42**(12): 969-978.

Peek, C. B., A. H. Affinati, K. M. Ramsey, H. Y. Kuo, W. Yu, L. A. Sena, O. Ilkayeva, B. Marcheva, Y. Kobayashi, C. Omura, D. C. Levine, D. J. Bacsik, D. Gius, C. B. Newgard, E. Goetzman, N. S. Chandel, J. M. Denu, M. Mrksich and J. Bass (2013). "Circadian clock NAD+ cycle drives mitochondrial oxidative metabolism in mice." Science **342**(6158): 1243417.
Rolfe, D. F. and G. C. Brown (1997). "Cellular energy utilization and molecular origin of standard metabolic rate in mammals." Physiol Rev **77**(3): 731-758.

Saltiel, A. R. and J. M. Olefsky (2017). "Inflammatory mechanisms linking obesity and metabolic disease." J Clin Invest **127**(1): 1-4.

Satapati, S., B. Kucejova, J. A. Duarte, J. A. Fletcher, L. Reynolds, N. E. Sunny, T. He, L. A. Nair, K. A. Livingston, X. Fu, M. E. Merritt, A. D. Sherry, C. R. Malloy, J. M. Shelton, J. Lambert, E. J. Parks, I. Corbin, M. A. Magnuson, J. D. Browning and S. C. Burgess (2016). "Mitochondrial metabolism mediates oxidative stress and inflammation in fatty liver." J Clin Invest **126**(4): 1605.

Temel, R. E., R. G. Lee, K. L. Kelley, M. A. Davis, R. Shah, J. K. Sawyer, M. D. Wilson and L. L. Rudel (2005). "Intestinal cholesterol absorption is substantially reduced in mice deficient in both ABCA1 and ACAT2." J Lipid Res **46**(11): 2423-2431.

Van Schaftingen, E., R. Rzem, A. Marbaix, F. Collard, M. Veiga-da-Cunha and C. L. Linster (2013). "Metabolite proofreading, a neglected aspect of intermediary metabolism." J Inherit Metab Dis **36**(3): 427-434.

Zhang, M., L. Li, W. Xie, J. F. Wu, F. Yao, Y. L. Tan, X. D. Xia, X. Y. Liu, D. Liu, G. Lan, M. Y. Zeng, D. Gong, H. P. Cheng, C. Huang, Z. W. Zhao, X. L. Zheng and C. K. Tang (2016). "Apolipoprotein A-1 binding protein promotes macrophage cholesterol efflux by facilitating apolipoprotein A-1 binding to ABCA1 and preventing ABCA1 degradation." Atherosclerosis **248**: 149-159.

CHAPTER 3

# Role of AIBP in Tumor Biology


## Abstract

AIBP acts as a suppressor of macrophage inflammation, a key factor in tumor growth and survival. Analysis of publically available sequencing data across multiple tumor types reveals that *Apoa1bp* is often upregulated in cancer. Additionally, AIBP mRNA and protein levels in commonly used cancer cell lines are high. We hypothesized that AIBP is pro-tumor, and mice lacking AIBP would be protected against tumor development. *Apoa1bp*$^{-/-}$ mice injected with B16 melanoma had increased tumor residency of inflammatory macrophages compared to C57BL/6 controls, as well as an increase in the ratio between inflammatory and repair macrophages. When injected with the carcinogen 3-methylcholanthrene (MCA), *de novo* tumor growth was slowed in *Apoa1bp*$^{-/-}$ mice. We conclude that absence of AIBP is protective against tumor growth.


## Introduction

Cancer is the second-leading cause of death in the United States, with 1.7 million new cases predicted to occur in 2018 alone (Siegel, Miller et al. 2018). While therapeutic advances have been made, many tumor types still offer poor prognosis for those diagnosed, and there is great interest in novel methods of tumor regulation. In solid tumors, high macrophage content is generally associated with a poor chance of survival (Ruffell and Coussens 2015). Modulation of tumor macrophages, especially by repolarization, is a promising therapeutic approach.

Tumor-associated macrophages (TAMs) are key players in the tumor microenvironment. Once present in the tumor, signals from both host and tumor cells shape the macrophage

functional phenotype. Macrophage polarization is important; M1 inflammatory macrophages are generally considered anti-tumor, while M2 macrophages provide tissue remodeling and tumor support (Mantovani and Allavena 2015). TAMs resemble M2 macrophages and are primarily supportive of tumor survival, secreting anti-inflammatory cytokines while promoting angiogenesis and metastasis (Chanmee, Ontong et al. 2014, Noy and Pollard 2014). Additionally, TAMs are poor antigen presenters and secrete CCL2 to recruit regulatory T cells, further dampening the anti-tumor immune response (Chanmee, Ontong et al. 2014).

Regulation of angiogenesis is critical to a tumor's survival, and has been linked to macrophage polarization. Vascularization allows oxygenation, nutrition, and removal of waste products, all necessary features for a tumor to thrive (Noy and Pollard 2014). As further evidence that M2 macrophages support tumor growth, increased vascularization and endothelial cell content was found in implanted Matrigel plugs supplemented with M2 macrophages compared to other subsets (Jetten, Verbruggen et al. 2014). Conversely, skewing TAMs to an M1 state promoted anti-tumor immune responses and inhibited tumor angiogenesis (Rolny, Mazzone et al. 2011).

TAMs are known to promote angiogenesis via secretion of VEGF-A (Riabov, Gudima et al. 2014). As a counter, AIBP has been shown to inhibit VEGF-mediated signaling by promoting cholesterol efflux from lipid rafts, thereby abolishing the VEGFR2 signaling platform (Fang, Choi et al. 2013). While the role of AIBP in tumor angiogenesis specifically has not been explored, it has been shown that *Apoa1bp*$^{-/-}$ mice have significantly increased vascularization of matrigel plugs, and increased blood vessel recovery in an ischemia model (Mao, Meng et al. 2017).

As a regulator of both macrophage inflammatory function and angiogenesis, AIBP may play a role in controlling tumor development and survival. We hypothesized that mice lacking AIBP, thus losing its pro-tumor suppression of macrophage inflammation, would be protected against tumor development.

## Methods

### *Cell culture*

B16 melanoma cells were a kind gift from Dr. Jack Bui. Cells were cultured in RPMI with supplementation of 10% heat-inactivated Fetal Bovine Serum (Omega Scientific), sodium bicarbonate, MEM NEAA, sodium pyruvate, gentamicin, and β-mercaptoethanol.

### *Animals and diets*

All animal experiments were conducted according to protocols approved by the Institutional Animal Care and Use Committee of the University of California, San Diego. Mice were housed up to 5 per standard cage at room temperature and maintained on a 12:12 hour light:dark cycle, with lights on at 07:00. Both food and water were available ad libitum. Wild type C57BL/6 mice were initially purchased from Jackson Lab (Bar Harbor, ME) and bred in-house for experiments. *Apoa1bp*$^{-/-}$ mice were generated in our group as previously described (Mao, Meng et al. 2017), mice develop and breed normally.

### *B16 implantation model*

B16 cells were released from tissue culture flasks with trypsin and suspended in complete media. Cells were washed three times with cold PBS and suspended in cold PBS at 5 million/mL for

injection. Mice were injected subcutaneously with 0.2mL cell suspension containing 1 million cells using a 25g needle.

*Tumor harvesting*

Mice were sacrificed by $CO_2$ inhalation and confirmed by cervical dislocation. Tumor was blunt dissected from mouse flank into petri dish and spleen was removed into separate dish. Tumor was minced finely in dish using two razor blades and 4mL HBSS was added before transfer to 15mL conical tube. Collagenase 0.5mL was added to minced tumor and incubated at 37C for 30 minutes, with agitation every 10 minutes. Spleen was homogenized in 3mL red cell lysis buffer by crushing between two frosted glass slides. Homogenate was transferred to a 15mL conical tube and allowed to settle. Top 2mL portion was transferred to a new tube for downstream FACS.

*Tumor FACS*

Tumor and spleen homogenates were spun and resuspended in 2mL HBSS and allowed to settle. Top 20uL was filtered into FACS tubes for staining. Fc block was added prior to staining. Antibodies used were MHCII-FITC, ICAM-PE, Ly6C-APC, 1A8-PE/Cy7, CD45-APC/Cy7, in 50uL total staining buffer. In some experiments CD11b-PE replaced ICAM-PE. Cells were incubated in staining 20 minutes on ice. Cells were washed and resuspended in 200uL staining buffer containing 7-AAD live/dead stain.

*CRISPR/Cas9*

Preparation of CRISPR/Cas9 nickase plasmids was performed as described by Ran et al. (Ran, Hsu et al. 2013). Plasmid backbone was ordered from Addgene (#92987). Insert oligos were designed using the DNA 2.0 online tool and ordered from Integrated DNA Technologies. Transfection was performed using Lipofectamine 3000 (Invitrogen) or nucleofection (Amaxa).

*MCA sarcomas*

Male mice were injected subcutaneously with either 25 or 50ug of 3-methylcholanthrene (MCA). Mice were monitored for weight and development of sarcomas. Tumors were measured multiple times per week using calipers. Mice were sacrificed when tumors reached 2cm in diameter. Upon sacrifice, tumors were homogenized as described for FACS but instead cultured for production of a cell line. Tumor slices were preserved in formal sucrose for sectioning or in RNAlater. One section per tumor was snap frozen in liquid nitrogen.

**Results**

*AIBP prevents inflammation in the tumor microenvironment*

Our experiments in chapter 1 showed that AIBP is able to regulate macrophage inflammation *in vitro*. As inflammation in the tumor microenvironment can be detrimental to its growth, we hypothesized that loss of AIBP would be protective in a cancer model. C57BL/6 and *Apoa1bp*$^{-/-}$ mice were injected subcutaneously with 1 million B16 melanoma cells and tumors were allowed to grow for either 7 or 10 days, depending on the experiment. Unexpectedly, there was a slight trend of increased tumor size in the *Apoa1bp*$^{-/-}$ mice (Figure 1A). Upon sacrifice tumors were excised and digested for FACS characterization of the immune profile. *Apoa1bp*$^{-/-}$ mice had significantly increased levels of inflammatory M1 macrophages in comparison to

C57BL/6 controls (Fig 1B). Additionally, the ratio of M1 to tumor-supportive M2 macrophages was greater in the knockouts, indicating less favorable conditions for tumor survival (Fig 1C).

*Tumors of different origins express varying levels of AIBP*

The experiments in Figure 1 employ knockout mice, but the B16 melanoma cells injected express an unknown amount of AIBP. In order to address this, four spontaneously developed sarcoma lines ("Bui") and two commonly used cancer lines were obtained. RNA was isolated from each and analyzed via qPCR to determine relative *Apoa1bp* expression, using primary mouse macrophages for reference. All lines had some expression, with Bui sarcoma 4862 and B16 melanoma having the highest levels (Fig 2A).

*Mice lacking AIBP are protected against tumor development*

Next, we set out to generate a cell line without AIBP expression by using CRISPR/Cas9. Two independent sets of nickase guideRNAs were designed and produced for use in the B16 melanoma line. However, while transfection efficiency was good, no knockout cell lines were generated after limiting dilution clonal expansion.

Instead of altering an existing cell line, we chose to produce our own line in mice lacking AIBP. This cell line could later have AIBP expression reintroduced, creating a matched set of lines for studying host versus tumor AIBP effects. To do this, we induced sarcoma development in C57BL/6 and *Apoa1bp*$^{-/-}$ mice using subcutaneous injection of 3-methylcholanthrene (MCA). Tumors were considered terminal when they reached 2cm in diameter. *Apoa1bp*$^{-/-}$ mice persisted longer before developing fatal tumors, and one mouse had a small tumor regress completely (Fig 2B).

**Discussion**

In this study, we explored the role of AIBP in the tumor immune contexture. We found that *Apoa1bp*$^{-/-}$ mice had increased tumor populations of inflammatory M1 macrophages in comparison to C57BL/6 mice, but were not protected against B16 melanoma tumor growth. In addition to its role in fighting developed tumors, we also examined how *Apoa1bp*$^{-/-}$ hosts survived under conditions of spontaneous sarcoma generation. Interestingly, *Apoa1bp*$^{-/-}$ mice reached a terminal tumor size later than controls, and one knockout mouse was deemed tumor-free at the end of the study.

One potential caveat to the B16 melanoma experiments performed here is that B16, like several other tumor lines, produces AIBP itself. This complicates experiments with knockout mice, as the tumor may be producing its own AIBP and negating the effects of the host environment. Interestingly, CRISPR/Cas9 deletion of AIBP in B16 melanoma resulted in no viable knockout cell lines, suggesting that the tumor may be dependent on its expression. Further work is necessary to determine if the tumor secretes AIBP, and if so what are its targets and functions.

While AIBP is a suppressor of inflammation, a pro-tumor function, its lipid raft-depleting mechanism regulates other cellular functions including angiogenesis. Tumors rely on blood vessels to provide oxygen and nutrients essential to their highly metabolic growth, meaning that AIBP-mediated suppression of angiogenesis is detrimental to the tumor. Whether the anti-angiogenic effects of AIBP outweigh its suppression of macrophage inflammation in the tumor microenvironment remains to be explored, and could be critical to the future implementation of AIBP therapy.

Our pilot study shows that AIBP plays a role in the tumor immune contexture and tumor development. We found that AIBP expression was present in all cultured tumor cell lines tested, however tumors were able to develop from cells lacking AIBP. The extent of AIBP's involvement in cancer is an important research area for future investigation.

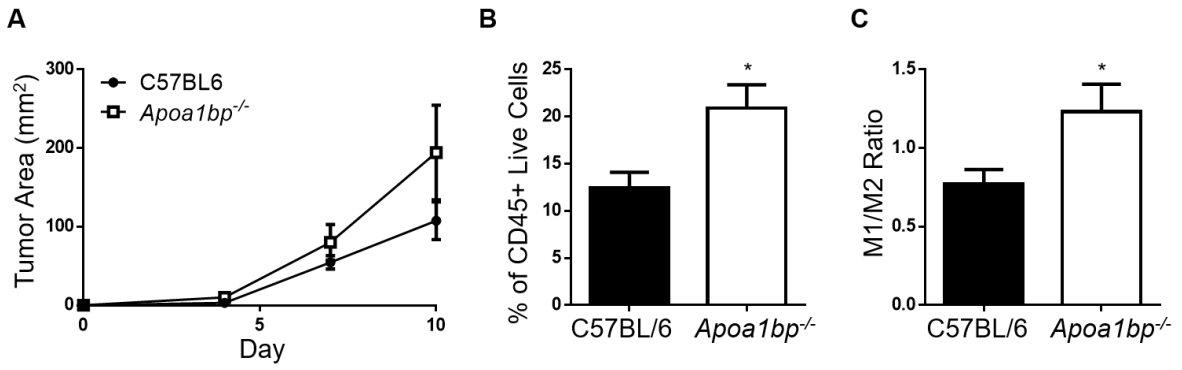


**Figure 3.1. Tumors in *Apoa1bp*$^{-/-}$ mice have increased inflammatory macrophage content.** A, Tumor growth curve. Mice were injected subcutaneously with 1 million B16 melanoma cells and tumor was allowed to grow. B, Tumor inflammatory macrophage content. Upon sacrifice, tumors were harvested and digested for FACS. Inflammatory M1 cells were considered CD45+MHCII$^{hi}$. C, Ratio of M1 to M2 macrophages. M2 cells were considered CD45+MHCII$^{lo}$. N=9-10, Mean±SEM; *,$p<0.05$ (t-test).

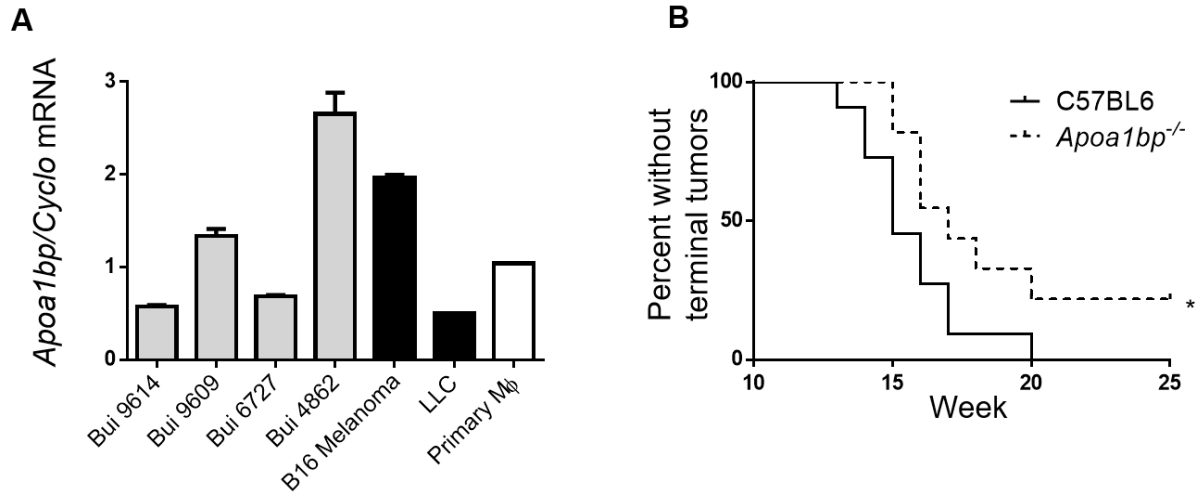


**Figure 3.2. *De novo* tumor AIBP expression and survival.** A, Expression of *Apoa1bp* in spontaneous sarcomas and tumor cell lines. RNA was isolated from MCA-induced sarcoma lines from the lab of Dr. Jack Bui (grey bars), commonly used cancer cell lines (black bars), and primary macrophages (white bar). Gene expression was normalized to cyclophilin. Statistics not performed. B, Terminal tumor curve of mice injected with MCA carcinogen. Tumors were considered terminal when diameter reached 2cm. N=11, Mean±SEM; *,$p<0.05$ (Gehan-Breslow-Wilcoxon test).

## Chapter References


Chanmee, T., P. Ontong, K. Konno and N. Itano (2014). "Tumor-associated macrophages as major players in the tumor microenvironment." Cancers (Basel) **6**(3): 1670-1690.

Fang, L., S. H. Choi, J. S. Baek, C. Liu, F. Almazan, F. Ulrich, P. Wiesner, A. Taleb, E. Deer, J. Pattison, J. Torres-Vazquez, A. C. Li and Y. I. Miller (2013). "Control of angiogenesis by AIBP-mediated cholesterol efflux." Nature **498**(7452): 118-122.

Jetten, N., S. Verbruggen, M. J. Gijbels, M. J. Post, M. P. De Winther and M. M. Donners (2014). "Anti-inflammatory M2, but not pro-inflammatory M1 macrophages promote angiogenesis in vivo." Angiogenesis **17**(1): 109-118.

Mantovani, A. and P. Allavena (2015). "The interaction of anticancer therapies with tumor-associated macrophages." J Exp Med **212**(4): 435-445.

Mao, R., S. Meng, Q. Gu, R. Araujo-Gutierrez, S. Kumar, Q. Yan, F. Almazan, K. A. Youker, Y. Fu, H. J. Pownall, J. P. Cooke, Y. I. Miller and L. Fang (2017). "AIBP Limits Angiogenesis Through gamma-Secretase-Mediated Upregulation of Notch Signaling." Circ Res.

Noy, R. and J. W. Pollard (2014). "Tumor-associated macrophages: from mechanisms to therapy." Immunity **41**(1): 49-61.

Ran, F. A., P. D. Hsu, J. Wright, V. Agarwala, D. A. Scott and F. Zhang (2013). "Genome engineering using the CRISPR-Cas9 system." Nat Protoc **8**(11): 2281-2308.

Riabov, V., A. Gudima, N. Wang, A. Mickley, A. Orekhov and J. Kzhyshkowska (2014). "Role of tumor associated macrophages in tumor angiogenesis and lymphangiogenesis." Front Physiol **5**: 75.

Rolny, C., M. Mazzone, S. Tugues, D. Laoui, I. Johansson, C. Coulon, M. L. Squadrito, I. Segura, X. Li, E. Knevels, S. Costa, S. Vinckier, T. Dresselaer, P. Akerud, M. De Mol, H. Salomaki, M. Phillipson, S. Wyns, E. Larsson, I. Buysschaert, J. Botling, U. Himmelreich, J. A. Van Ginderachter, M. De Palma, M. Dewerchin, L. Claesson-Welsh and P. Carmeliet (2011). "HRG inhibits tumor growth and metastasis by inducing macrophage polarization and vessel normalization through downregulation of PlGF." Cancer Cell **19**(1): 31-44.

Ruffell, B. and L. M. Coussens (2015). "Macrophages and therapeutic resistance in cancer." Cancer Cell **27**(4): 462-472.

Siegel, R. L., K. D. Miller and A. Jemal (2018). "Cancer statistics, 2018." CA Cancer J Clin **68**(1): 7-30.